JM PAPERS

Resistance and mobility functions for the near-contact motion of permeable particles

Rodrigo B. Reboucas[1] **and Michael Loewenberg** [1],†

[1]Department of Chemical and Environmental Engineering, Yale University, New Haven, CT 06520-8286, USA

A lubrication analysis is presented for the resistances between permeable spherical particles in near contact, $h_0/a \ll 1$, where h_0 is the minimum separation between the particles, and $a = a_1 a_2/(a_1 + a_2)$ is the reduced radius. Darcy's law is used to describe the flow inside the permeable particles and no-slip boundary conditions are applied at the particle surfaces. The weak permeability regime $K = k/a^2 \ll 1$ is considered, where $k = \frac{1}{2}(k_1 + k_2)$ is the mean permeability. Particle permeability enters the lubrication resistances through two functions of $q = K^{-2/5}h_0/a$, one describing axisymmetric motions, the other transverse. These functions are obtained by solving an integral equation for the pressure in the near-contact region. The set of resistance functions thus obtained provide the complete set of near-contact resistance functions for permeable spheres and match asymptotically to the standard hard-sphere resistances that describe pairwise hydrodynamic interactions away from the near-contact region. The results show that permeability removes the contact singularity for non-shearing particle motions, allowing rolling without slip and finite separation velocities between touching particles. Axisymmetric and transverse mobility functions are presented that describe relative particle motion under the action of prescribed forces and in linear flows. At contact, the axisymmetric mobility under the action of oppositely directed forces is $U/U_0 = d_0 K^{2/5}$, where U is the relative velocity, U_0 is the velocity in the absence of hydrodynamic interactions and $d_0 = 1.332$. Under the action of a constant tangential force, a particle in contact with a permeable half-space rolls without slipping with velocity $U/U_0 = d_1(d_2 + \log K^{-1})^{-1}$, where $d_1 = 3.125$ and $d_2 = 6.666$; in shear flow, the same expression holds with $d_1 = 7.280$.

Key words: lubrication theory, porous media

† Email address for correspondence: michael.loewenberg@yale.edu

1. Introduction

Understanding particle filtration and particle flocculation require an understanding of the hydrodynamic interactions of permeable particles and particles with a permeable medium (Belfort, Davis & Zydney 1994; Le-Clech, Chen & Fane 2006; Civan 2007; Hwang & Sz 2011; Wang *et al.* 2020). The operation and design of packed-bed and fluidized reactors (Rodrigues, Ahn & Zoulalian 1982; Davis & Stone 1993) and chromatography columns (Liapis & McCoy 1994; Blue & Jorgenson 2015) also relies on a fundamental understanding of the hydrodynamics of permeable particles.

Fluid flow in a homogeneous, permeable material is usually described using Darcy's law (Darcy 1856), whereby the fluid velocity $\boldsymbol{v}$ in a permeable medium is given by

$$\boldsymbol{v} = -\frac{k}{\mu}\boldsymbol{\nabla}p, \tag{1.1}$$

where k is the permeability, μ is the fluid viscosity and $\boldsymbol{\nabla}p$ is the local pressure gradient. The permeability scales with the square of the pore size and Darcy's law is appropriate when the length scale set by pressure gradients is much larger than the pore scale. The normal velocity and pressure are continuous at the boundary of a permeable material and the free fluid region. There have been several investigations of the appropriate boundary condition for the tangential velocity (Beavers & Joseph 1967; Saffman 1971; Neale & Nader 1974; Ochoa-Tapia & Whitaker 1995; Bars & Woster 2006; Cao *et al.* 2010) but the no-slip boundary condition is most frequently used.

Brinkman's equation (Brinkman 1949) is another widely used description of flows in permeable media. However, it is physically justified only for materials with very sparse microstructures, consisting of fixed arrays of particles (Tam 1969; Childress 1972; Howells 1974; Lévy 1983), e.g. arrays of spheres with at least 95 % porosity (Durlofsky & Brady 1987). In any case, the 'Brinkman term' (i.e. Laplacian of the velocity) has an $O(k/L^2)$ relative magnitude, where L is the length scale associated with velocity gradients and $k^{1/2}$ is the pore scale. Accordingly, Brinkman's equation often reduces to Darcy's law, given that $L \gg k^{1/2}$ usually applies (Auriault 2009). As shown below, these conditions apply for the near-contact motion of permeable particles.

Hydrodynamic interactions between spherical particles and thin, permeable layers have been analysed as a model for filtration (Goren 1979; Nir 1981; Debbech, Elasmi & Feuillebois 2010; Ramon & Hoek 2012; Ramon *et al.* 2013; Khabthani, Sellier & Feuillebois 2019). Several studies explored the hydrodynamic interactions of spherical particles with permeable half-spaces (Michalopoulou, Burganos & Payatakes 1992; Damiano *et al.* 2004), conversely, others considered the interactions of permeable spheres with impermeable walls (Payatakes & Dassios 1987; Burganos *et al.* 1992; Davis 2001; Roy & Damiano 2008), and a few analysed hydrodynamic interactions between pairs of permeable spheres (Jones 1978; Michalopoulou, Burganos & Payatakes 1993; Bäbler *et al.* 2006). Creeping flow conditions were assumed in all of these studies. Some used Darcy's law to describe the fluid flow in the permeable medium, others used Brinkman's equation (despite its limitations discussed above), the choice usually related to the porosity of the material (Auriault 2009). Most of the prior studies consider axisymmetric motion and the results show that permeability reduces hydrodynamic resistance (Goren 1979; Nir 1981; Payatakes & Dassios 1987; Burganos *et al.* 1992; Michalopoulou *et al.* 1992, 1993; Davis 2001; Debbech *et al.* 2010; Ramon & Hoek 2012; Ramon *et al.* 2013; Khabthani *et al.* 2019).

Much more is known about pairwise hydrodynamic interactions of hard spheres, i.e. impermeable rigid spheres, in creeping flows. Beginning with the classical study on

axisymmetric pair interactions by Stimson & Jeffery (1926), a complete formal framework was developed for pair interactions (Cooley & O'Neill 1969*a*; Lin, Lee & Sather 1970; O'Neill & Majumdar 1970*a,b*; Batchelor & Green 1972; Brenner & O'Neill 1972; Nir & Acrivos 1973; Batchelor 1982; Jeffrey 1982; Jeffrey & Onishi 1984*a,b*; Kim & Mifflin 1985; Corless & Jeffrey 1988*a,b*; Jeffrey 1989, 1992) with several additional studies on particle–wall interactions (Brenner 1961; Maude 1963; Goldman, Cox & Brenner 1967*a,b*; O'Neill & Stewartson 1967; Cooley & O'Neill 1968). This work is summarized in classic texts (Happel & Brenner 1983; Kim & Karrila 2005). A principal result from this body of research is the general relationship between the forces, torques and stresslets acting on the particles and their linear and angular velocities and the imposed stress field by a grand resistance matrix that involves a set of scalar resistance functions that depend only on the centre-to-centre distance between particles (Kim & Karrila 2005).

Several methods have been used to compute the pairwise hydrodynamic resistances of hard spheres. Calculations using bispherical coordinates (Stimson & Jeffery 1926; Brenner 1961; Lin *et al.* 1970; O'Neill & Majumdar 1970*a*; Ingber & Zinchenko 2012), twin-multipole expansions (Jeffrey & Onishi 1984*a,b*; Jeffrey 1992) and boundary collocation (Kim & Mifflin 1985) provide exact results for all but near-contact configurations with vanishing surface-to-surface separation, $h_0 \to 0$, where the resistances are singular and these methods fail. The contact singularities of the resistance functions control important qualitative features of the hard-sphere dynamics. An example is the classical result that hard spheres cannot be pushed into contact by a finite force and thus interparticle contact does not occur in hard-sphere suspensions without singular interparticle forces (e.g. van der Waals attraction). Near-contact resistances must therefore be resolved, usually by a lubrication analysis (Goldman *et al.* 1967*a,b*; O'Neill & Stewartson 1967; Cooley & O'Neill 1968; O'Neill & Majumdar 1970*b*; Jeffrey 1982; Corless & Jeffrey 1988*a,b*; Jeffrey 1989).

The same methods have been applied to problems involving permeable particles and/or boundaries. Several studies on axisymmetric motion used bispherical coordinates calculations (Goren 1979; Payatakes & Dassios 1987; Burganos *et al.* 1992; Michalopoulou *et al.* 1992, 1993; Davis 2001), and a few others used boundary collocation (Chen 1998; Chen & Cai 1999). Prior lubrication analyses have focused on the axisymmetric near-contact motion of hard spheres with permeable membranes. In a recent analysis of the near-contact motion between permeable spheres, we showed that the lubrication resistance between permeable particles is non-singular at contact, in contrast to the $O(a/h_0)$ lubrication singularity that characterizes the relative motion of hard spheres (Reboucas & Loewenberg 2021*a*). This feature allows contact between particles in suspension, even without the presence of interparticle forces (Reboucas & Loewenberg 2021*b*).

Here, we extend our previous lubrication analysis (Reboucas & Loewenberg 2021*a*) to the case of asymmetric, transverse motion and use the general resistance framework for spherical particles (Kim & Karrila 2005) to derive the complete set of resistance functions that describe the near-contact motion of rigid, permeable spheres. The intraparticle flow is governed by Darcy's law, no-slip boundary conditions are applied on the particle surfaces and weak permeability conditions are assumed,

$$K \ll 1, \tag{1.2}$$

where $K = k/a^2$ is the dimensionless permeability, k is the arithmetic mean permeability of the particles,

$$k = \tfrac{1}{2} (k_1 + k_2) \tag{1.3}$$

and $a = a_1 a_2 (a_1 + a_2)^{-1}$ is the reduced radius; subscripts 1 and 2 are particle labels. As discussed above, Brinkman's equation is inappropriate under weak permeability conditions. However, the use of Brinkman's equation would not significantly influence the results presented here because the length scale associated with the intraparticle velocity has the lower bound $L \geq k^{1/5} a^{3/5}$ (Reboucas & Loewenberg 2021*a*) thus, the Brinkman term has a sub-dominant, $O(K^{3/5})$, relative magnitude in Brinkman's equation (Auriault 2009).

Under weak permeability conditions (1.2), hydrodynamic resistances are sensitive to the permeability, and qualitatively affected, for gap widths $h_0/a = O(K^{2/5})$, but at larger separations, particle permeability has a much weaker $O(K)$ effect on hydrodynamic resistances, allowing permeable particles to be approximated by hard spheres away from the near-contact region (Reboucas & Loewenberg 2021*a*). Thus, combining the lubrication resistances presented here with the resistances for well-separated hard spheres tabulated in the literature (Kim & Karrila 2005) provides a complete hydrodynamic description for pairwise hydrodynamic interactions of permeable spheres.

The governing lubrication equations are derived in § 2. An integral Reynolds lubrication equation that governs the pressure distribution is derived and solved numerically in § 3. The formulation allows for arbitrary ratios of particle radii and particles with different permeabilities. The resistance functions that describe the near-contact motion of permeable spheres are presented in § 4. Mobility functions, derived by combining the lubrication resistance functions for permeable spheres with the hard-sphere hydrodynamic functions for $h_0/a \gg K^{2/5}$, are presented in § 5, including the special case of a particle undergoing near-contact translation parallel to a wall or a permeable half-space under the action of an applied force or an imposed shear flow. Concluding remarks are presented in § 6.

2. Problem formulation

The transverse motion of two permeable spheres separated by a small gap h_0 in a fluid with viscosity μ is considered here. Particle 1 has radius a_1, particle 2 has radius a_2 and $\kappa = a_2/a_1$ will be used to denote the size ratio.

Note that various symbols have been used to denote size ratio in prior lubrication analyses, e.g. $k^{-1} = |a_2/a_1|$ (O'Neill & Majumdar 1970*b*), $\kappa = -a_1/a_2$ (Jeffrey 1982; Corless & Jeffrey 1988*a*,*b*), $\lambda = a_2/a_1$ (Batchelor 1982; Jeffrey & Onishi 1984*a*; Jeffrey 1989, 1992) and $\beta = a_2/a_1$ (Kim & Karrila 2005). We use $\kappa = a_2/a_1$ here for consistency with our earlier study (Reboucas & Loewenberg 2021*a*).

2.1. *Lubrication equations for transverse motions of permeable particles*

A cylindrical coordinate system (r, θ, z) is used with z-coordinate coincident with the line of centres of the two particles, and with $z = 0$ at the surface of particle 2 shown in figure 1. A Cartesian coordinate system (x, y, z) is also defined with the same origin, x-coordinate aligned with $\theta = 0$, and y aligned with $\theta = \pi/2$. The surfaces of the particles are approximately parabolic in the near-contact region, $r \ll a$, where $a = a_1 a_2/(a_1 + a_2)$ is the reduced radius. The surface of particle 1 corresponds to $z = h_0 + r^2/(2a_1)$, and the surface of particle 2 corresponds to $z = -r^2/(2a_2)$.

The leading-order lubrication equations for transverse motion of the particles are

$$\frac{\partial^2 \bar{v}_r}{\partial \bar{z}^2} = \frac{\partial \bar{p}}{\partial \bar{r}}, \quad \frac{\partial^2 \bar{v}_\theta}{\partial \bar{z}^2} = \frac{1}{\bar{r}} \frac{\partial \bar{p}}{\partial \theta}, \quad \frac{\partial \bar{p}}{\partial \bar{z}} = 0, \quad \frac{1}{\bar{r}} \frac{\partial}{\partial \bar{r}} (\bar{r} \bar{v}_r) + \frac{1}{\bar{r}} \frac{\partial \bar{v}_\theta}{\partial \theta} + \frac{\partial \bar{v}_z}{\partial \bar{z}} = 0. \quad (2.1a\text{–}d)$$
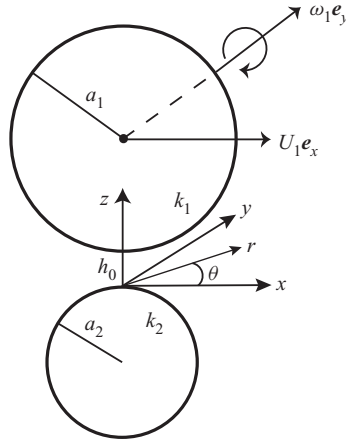
Figure 1. Schematic showing two particles with radii and permeabilities a_i and k_i ($i = 1, 2$), respectively, separated by a gap h_0; particle 1 has translational and angular velocities U_1 and ω_1; particle 2 is stationary. The Cartesian and cylindrical coordinate systems are shown.

The overbars denote dimensionless variables defined by

$$\bar{r} = \frac{r}{L_1}, \quad \bar{z} = \frac{za_1}{L_1^2}, \quad \bar{v}_r = \frac{v_r}{U_0}, \quad \bar{v}_\theta = \frac{v_\theta}{U_0}, \quad \bar{w} = \frac{wa_1}{U_0 L_1}, \quad \bar{p} = \frac{pL_1^3}{\mu U_0 a_1^2}, \quad (2.2a\text{–}f)$$

where $L_1 = \sqrt{a_1 h_0}$ is the characteristic lateral length scale set by the geometry of the near-contact region, and U_0 is a characteristic velocity magnitude that depends on the boundary conditions of the problem. The lubrication approximation holds when $h_0 \ll a$.

Only two transverse motions need consideration: (a) transverse motion of particle 1 with velocity in the x-direction (i.e. $\theta = 0$) with magnitude U_1, and (b) rotation of particle 1 with angular velocity in the positive y-direction with magnitude ω_1. Particle 2 is stationary in both problems. The resistances corresponding to the translation and rotation of particle 2 are obtained by relabelling and symmetry. Boundary conditions for these two problems are

$$\bar{z} = \bar{z}_1(\bar{r}) : \begin{cases} \bar{v}_r = (\bar{U}_1 - \bar{\omega}_1)\cos\theta, \quad \bar{v}_\theta = -(\bar{U}_1 - \bar{\omega}_1)\sin\theta \\ \bar{v}_z = -\bar{\omega}_1 \bar{r}\cos\theta + \bar{j}_1[\bar{p}](\bar{r}, \theta) \end{cases}, \quad (2.3)$$

$$\bar{z} = \bar{z}_2(\bar{r}) : \quad \bar{v}_r = \bar{v}_\theta = 0, \quad \bar{v}_z = -\bar{j}_2[\bar{p}](\bar{r}, \theta), \quad (2.4)$$

where $\bar{z}_1$ and $\bar{z}_2$ define the surfaces of particles 1 and 2, respectively,

$$\bar{z}_1 = 1 + \frac{1}{2}\bar{r}^2, \quad \bar{z}_2 = -\frac{1}{2\kappa}\bar{r}^2. \quad (2.5a,b)$$

Here, $\bar{U}_1 = U_1/U_0$ and $\bar{\omega}_1 = \omega_1 a_1/U_0$ are the dimensionless translational and rotational velocities of particle 1. Recall that $\kappa = a_2/a_1$.

The quantities j_1, j_2 are the fluxes of fluid into the surfaces of the permeable particles. Given that the intraparticle pressure fields satisfy Laplace's equation, are equal to the lubrication pressure at the particle surfaces, and decay to zero inside the particles, as shown in Appendix A, it follows that the intraparticle fluxes are linear functionals of the lubrication pressure. The intraparticle fluxes are normal to the particle surfaces but, as discussed in Appendix A, act in the z-direction to leading order, and thus only enter

the boundary condition for the velocity in the z-direction, as indicated in (2.3)–(2.4). The fluxes are made dimensionless by the characteristic velocity in the z-direction, $U_0 L_1 / a_1$,

$$\bar{j}_i = \frac{j_i a_1}{U_0 L_1}, \quad i = 1, 2. \tag{2.6}$$

Boundary conditions (2.3)–(2.4) impose the following θ-dependence:

$$\bar{v}_r = \bar{U}(\bar{r}, \bar{z}) \cos \theta, \quad \bar{v}_\theta = \bar{V}(\bar{r}, \bar{z}) \sin \theta, \quad \bar{v}_z = \bar{W}(\bar{r}, \bar{z}) \cos \theta, \tag{2.7a}$$

$$\bar{p} = \bar{P}(\bar{r}) \cos \theta, \quad \bar{j}_i = \bar{J}_i[\bar{P}](\bar{r}) \cos \theta, \quad i = 1, 2. \tag{2.7b}$$

Inserting these forms into the lubrication equations (2.1a–d) and boundary conditions (2.3)–(2.4) yields,

$$\frac{\partial^2 \bar{U}}{\partial \bar{z}^2} = \bar{P}', \quad \frac{\partial^2 \bar{V}}{\partial \bar{z}^2} = -\frac{\bar{P}}{\bar{r}}, \tag{2.8a,b}$$

$$\frac{\partial \bar{U}}{\partial \bar{r}} + \frac{1}{\bar{r}} \left(\bar{U} + \bar{V} \right) + \frac{\partial \bar{W}}{\partial \bar{z}} = 0, \tag{2.9}$$

$$\bar{z} = \bar{z}_1(\bar{r}) : \begin{cases} \bar{U} = (\bar{U}_1 - \bar{\omega}_1), \quad \bar{V} = -(\bar{U}_1 - \bar{\omega}_1), \\ \bar{W} = -\bar{\omega}_1 \bar{r} + \bar{J}_1[\bar{P}](\bar{r}). \end{cases} \tag{2.10}$$

$$\bar{z} = \bar{z}_2(\bar{r}) : \quad \bar{U} = \bar{V} = 0, \quad \bar{W} = -\bar{J}_2[P](\bar{r}). \tag{2.11}$$

Note that $\bar{P}$ depends only on $\bar{r}$, and the prime in (2.8a,b) denotes a derivative. Integrating the (2.8a,b) with boundary conditions (2.10)–(2.11) for $\bar{U}$ and $\bar{V}$ yields

$$\bar{U} = \frac{1}{2} \bar{P}'(\bar{r})(\bar{z} - \bar{z}_1(\bar{r}))(\bar{z} - \bar{z}_2(\bar{r})) + \frac{\bar{U}_1 - \bar{\omega}_1}{\bar{h}(\bar{r})} (\bar{z} - \bar{z}_2(\bar{r})), \tag{2.12a}$$

$$\bar{V} = -\frac{1}{2\bar{r}} \bar{P}(\bar{r})(\bar{z} - \bar{z}_1(\bar{r}))(\bar{z} - \bar{z}_2(\bar{r})) - \frac{\bar{U}_1 - \bar{\omega}_1}{\bar{h}(\bar{r})} (\bar{z} - \bar{z}_2(\bar{r})), \tag{2.12b}$$

where

$$\bar{h}(\bar{r}) = \bar{z}_1 - \bar{z}_2 = 1 + \tfrac{1}{2}(1 + \kappa^{-1}) \bar{r}^2. \tag{2.13}$$

Inserting these results into the continuity equation (2.9) and integrating using the boundary conditions for $\bar{W}$, yields the Reynolds lubrication equation

$$\frac{1}{12\bar{r}} \left(\bar{r} \bar{P}' \bar{h}^3 \right)' - \frac{1}{12\bar{r}^2} \bar{P} \bar{h}^3 - 2\bar{J}[\bar{P}] = -\frac{1}{2} C \left(1 + \kappa^{-1} \right) \bar{r}, \tag{2.14a}$$

which satisfies the homogeneous boundary conditions

$$\bar{P}(0) = \bar{P}(\infty) = 0. \tag{2.14b}$$

Here, primes are used to denote differentiation with respect to $\bar{r}$ and C is the constant

$$C = \left[(\bar{U}_1 + \bar{\omega}_1) - \kappa^{-1} (\bar{U}_1 - \bar{\omega}_1) \right] \left(1 + \kappa^{-1} \right)^{-1}. \tag{2.15}$$

The quantity $2\bar{J} = \bar{J}_1 + \bar{J}_2$ is the combined flux into both particles. For hard spheres, i.e. $\bar{J} = 0$, the solution of (2.14) is

$$\bar{P}_\infty(\kappa, \bar{r}) = C \frac{6}{5} \frac{\bar{r}}{\bar{h}^2}. \tag{2.16}$$

2.2. *Forces, torques and stresslets*

The forces, torques and stresslets on each of the spheres are calculated using the relations (O'Neill & Majumdar 1970*b*; Corless & Jeffrey 1988*b*),

$$
\frac{F_{x_1}}{\pi \mu U_0 a_1} = \int_0^{\bar{R}_0} \left[-\bar{P}r + \left(\frac{\partial \bar{V}}{\partial \bar{z}} - \frac{\partial \bar{U}}{\partial \bar{z}} \right)_{\bar{z}=\bar{z}_1} \right] r \, dr, \tag{2.17}
$$

$$
\frac{F_{x_2}}{\pi \mu U_0 a_1} = \int_0^{\bar{R}_0} \left[-\bar{P}r\kappa^{-1} + \left(\frac{\partial \bar{U}}{\partial \bar{z}} - \frac{\partial \bar{V}}{\partial \bar{z}} \right)_{\bar{z}=\bar{z}_2} \right] r \, dr, \tag{2.18}
$$

$$
\frac{T_{y_1}}{\pi \mu U_0 a_1^2} = \int_0^{\bar{R}_0} \left(\frac{\partial \bar{U}}{\partial \bar{z}} - \frac{\partial \bar{V}}{\partial \bar{z}} \right)_{\bar{z}=\bar{z}_1} r \, dr, \tag{2.19}
$$

$$
\frac{T_{y_2}}{\pi \mu U_0 a_1^2} = \kappa \int_0^{\bar{R}_0} \left(\frac{\partial \bar{U}}{\partial \bar{z}} - \frac{\partial \bar{V}}{\partial \bar{z}} \right)_{\bar{z}=\bar{z}_2} r \, dr, \tag{2.20}
$$

$$
\frac{S_{xz,1}}{\pi \mu U_0 a_1^2} = \int_0^{\bar{R}_0} \left[\bar{P}r + \frac{1}{2} \left(\frac{\partial \bar{U}}{\partial \bar{z}} - \frac{\partial \bar{V}}{\partial \bar{z}} \right)_{\bar{z}=\bar{z}_1} \right] r \, dr, \tag{2.21}
$$

$$
\frac{S_{xz,2}}{\pi \mu U_0 a_1^2} = \int_0^{\bar{R}_0} \left[-\bar{P}r + \frac{\kappa}{2} \left(\frac{\partial \bar{U}}{\partial \bar{z}} - \frac{\partial \bar{V}}{\partial \bar{z}} \right)_{\bar{z}=\bar{z}_2} \right] r \, dr, \tag{2.22}
$$

where the upper limit of integration is $\bar{R}_0 = O(\sqrt{a_1/h_0})$, a precise definition is not required (O'Neill & Stewartson 1967; Kim & Karrila 2005).

Inserting (2.12*a,b*) into (2.17)–(2.22) and integrating by parts to separate the pressure contributions yields

$$
\frac{F_{x_1}}{\pi \mu U_0 a_1} = \frac{1}{2} C \left(\kappa^{-1} - 1 \right) (I_1 - I_K) - 2BI_2, \tag{2.23}
$$

$$
\frac{F_{x_2}}{\pi \mu U_0 a_1} = -\frac{1}{2} C \left(\kappa^{-1} - 1 \right) (I_1 - I_K) + 2BI_2, \tag{2.24}
$$

$$
\frac{T_{y_1}}{\pi \mu U_0 a_1^2} = -\frac{1}{2} C \left(1 + \kappa^{-1} \right) (I_1 - I_K) + 2BI_2, \tag{2.25}
$$

$$
\frac{T_{y_2}}{\pi \mu U_0 a_1^2} = \frac{1}{2} C \left(1 + \kappa \right) (I_1 - I_K) + 2\kappa BI_2, \tag{2.26}
$$

$$
\frac{S_{xz,1}}{\pi \mu U_0 a_1^2} = \frac{1}{4} C \left(3 - \kappa^{-1} \right) (I_1 - I_K) + BI_2, \tag{2.27}
$$

$$
\frac{S_{xz,2}}{\pi \mu U_0 a_1^2} = -\frac{1}{4} C (3 - \kappa)(I_1 - I_K) + \kappa BI_2, \tag{2.28}
$$

where B is given by

$$
B = \bar{U}_1 - \bar{\omega}_1 \tag{2.29}
$$

and C is defined by (2.15). Here, we define the integrals

$$
I_1(\xi, \kappa, \bar{R}_0) = \int_0^{\bar{R}_0} \bar{\mathcal{P}}_\infty r^2 \, dr, \quad I_2(\xi, \kappa, \bar{R}_0) = \int_0^{\bar{R}_0} \frac{r}{\bar{h}} \, dr, \tag{2.30a,b}
$$

and

$$I_K(\xi, \kappa, K) = \int_0^\infty (\bar{\mathcal{P}}_\infty - \bar{\mathcal{P}})r^2 \, \mathrm{d}r, \tag{2.31}$$

where $\xi = h_0/\bar{a}$ is the gap normalized by the average radius, and $\kappa = a_2/a_1$ is the size ratio. Here, $\mathcal{P}$ is the rescaled pressure

$$P = C\mathcal{P}, \tag{2.32}$$

which is introduced for convenience in the solution of the Reynolds lubrication equation that follows below.

This rearrangement of (2.17)–(2.22) is useful because it isolates the influence of particle permeability. The integrals I_1 and I_2 describe the dynamics of hard spheres; only the permeability integral, I_K, depends on the permeability. The upper limit for I_K can be extended to infinity because $\bar{\mathcal{P}}_\infty - \bar{\mathcal{P}}$ decays sufficiently fast for $\bar{r} \to \infty$, indicating that permeability does not affect flow in the matching region.

3. Solution of the Reynolds equation

In this section, an integral equation is derived for the pressure that allows evaluation of the permeability integral, I_K. Numerical and asymptotic limiting results are presented. As shown below, the permeability integral can be expressed in terms of a single-variable permeability function

$$I_K(\xi, \kappa, K) = \left(1 + \kappa^{-1}\right)^{-2} g(q), \tag{3.1}$$

where the parameter q is defined

$$q = K^{-2/5} \frac{h_0}{a}. \tag{3.2}$$

Here, K is the dimensionless permeability,

$$K = k/a^2, \tag{3.3}$$

where $k = \frac{1}{2}(k_1 + k_2)$ is the mean permeability, and $a = a_1 a_2/(a_1 + a_2)$ is the reduced radius.

To obtain the functional form (3.1), we rescale the lubrication equation (2.14) using the variables

$$\hat{r} = \frac{r}{L_0}, \quad \hat{z} = \frac{za}{L_0^2}, \quad \hat{P} = \frac{pL_0^3}{\mu U_0 a^2}, \quad \hat{J} = \frac{Ja}{U_0 L_0} q^{5/2}, \tag{3.4a–d}$$

where

$$L_0 = \sqrt{ah_0}, \tag{3.5}$$

is the length scale set by the geometry of the near-contact region (2.13), and a is the reduced radius. The scaling for the particle flux is obtained using the order-of-magnitude estimate, $J \sim kp/\mu L_0$ where $p \sim \mu U_0 a^2/L_0^3$ is the magnitude of pressure in the near-contact region.

In terms of these variables, the Reynolds lubrication equation (2.14) transforms to a one-parameter equation, depending only on q. The result is

$$\frac{1}{12\hat{r}}\left(\hat{r}\hat{\mathcal{P}}'\hat{h}^3\right)' - \frac{1}{12\hat{r}^2}\hat{\mathcal{P}}\hat{h}^3 - 2q^{-5/2}\hat{J}\left[\hat{\mathcal{P}}\right] = -\frac{1}{2}\hat{r}, \tag{3.6a}$$

with boundary conditions

$$\hat{\mathcal{P}}(0) = \hat{\mathcal{P}}(\infty) = 0, \tag{3.6b}$$

where

$$\hat{h}(\hat{r}) = 1 + \tfrac{1}{2}\hat{r}^2 \tag{3.7}$$

is the gap profile, and primes denote differentiation with respect to $\hat{r}$.

As shown in Appendix A, the intraparticle flux depends only on the mean permeability (1.3) and is expressed as a boundary integral of the pressure distribution in the gap between the particles

$$\hat{J}[\hat{\mathcal{P}}](\hat{r}) = -\int_0^\infty \hat{w}(r)\phi\left(r/\hat{r}\right)\mathrm{d}r, \tag{3.8}$$

where $\hat{w}$ is defined by derivatives of the pressure

$$\hat{w}(\hat{r}) = \left[\frac{1}{\hat{r}}\left(\hat{r}\hat{\mathcal{P}}\right)'\right]', \tag{3.9}$$

and the Green's function, $\phi(x)$, is given by (A15). Similar boundary integrals arise in analogous lubrication problems from other fields where a coupling exists between spheres in contact, or near contact, and intraparticle transport (Hertz 1882; Batchelor & O'Brien 1977; Davis, Schonberg & Rallison 1989).

The integro-differential Reynolds equation (3.6a) can be reduced to the integral equation,

$$\tfrac{1}{12}\hat{w}\hat{h}^3 + \tfrac{1}{4}\left(\hat{I}_A\left[\hat{w}\right] + \hat{I}_B\left[\hat{w}\right]\right)\hat{h}^2\hat{r} - 2q^{-5/2}\hat{J}\left[\hat{w}\right] = -\tfrac{1}{2}\hat{r}, \tag{3.10}$$

where boundary conditions (3.6a) are incorporated, $\hat{w}$ is defined by (3.9) and

$$\hat{I}_A\left[\hat{w}\right] = -\frac{1}{2}\int_{\hat{r}}^\infty \hat{w}\,\mathrm{d}r, \quad \hat{I}_B\left[\hat{w}\right] = \frac{1}{2}\int_0^{\hat{r}}\left(\frac{r}{\hat{r}}\right)^2\hat{w}\,\mathrm{d}r. \tag{3.11a,b}$$

The rescaled pressure is obtained as

$$\hat{\mathcal{P}} = \left(\hat{I}_A - \hat{I}_B\right)\hat{r}. \tag{3.12}$$

The permeability function (3.1) is given by

$$g(q) = \int_0^\infty (\hat{\mathcal{P}}_\infty - \hat{\mathcal{P}})r^2\,\mathrm{d}r, \tag{3.13}$$

which, after integration by parts, becomes

$$g(q) = \frac{1}{8}\int_0^\infty (\hat{w}_\infty - \hat{w})r^4\,\mathrm{d}r. \tag{3.14}$$

Here, $\hat{\mathcal{P}}_\infty$ is the pressure for hard spheres (2.16)

$$\hat{\mathcal{P}}_\infty(\hat{r}) = \frac{6}{5}\frac{\hat{r}}{\hat{h}^2}, \tag{3.15}$$

and

$$\hat{w}_\infty(\hat{r}) = \hat{w}\left[\hat{\mathcal{P}}_\infty\right](\hat{r}) = \frac{12\hat{r}}{5}\frac{\hat{r}^2 - 4}{\hat{h}^4}. \tag{3.16}$$

3.1. *Numerical method*

Integral (3.10), was discretized on a set of N points using a uniform mesh $\hat{r}_i$, ($i = 1, \ldots, N$) on the interval $0 \leq \hat{r} \leq \hat{r}_N$. An $N \times N$ system of equations was thus generated for the values $\hat{w}_i$ at each of the points $\hat{r}_i$ using a piecewise linear representation of $\hat{w}$. The non-singular integrals $\hat{I}_A$ and $\hat{I}_B$, respectively, yield upper and lower triangular matrices with elements evaluated by trapezoid-rule integration on the intervals between points. The matrix obtained by discretizing the flux integral (3.8) was obtained by analytically evaluating the log-singular portion of the Green's function (A20) on all intervals and evaluating the non-analytic remainder with adaptive Gaussian quadratures. This method yields $O(1/N^2)$ convergence, and the permeability function $g(q)$ was obtained to $O(1/N^3)$ accuracy by extrapolating for $N \to \infty$ using results from calculations with different numbers of points. The contributions to integrals from the region $\hat{r}_N \leq \hat{r} \leq \infty$ were approximately incorporated using $\hat{w} \approx \hat{w}_\infty$ for $\hat{r} > \hat{r}_N$ to accelerate the convergence for $\hat{r}_N \to \infty$. The system of equations were iteratively solved using a Gauss–Seidel scheme.

The numerical values provided in the Supplementary Material available at https://doi.org/10.1017/jfm.2022.171 were obtained from calculations with $N \approx 400$ and $\hat{r}_N \approx 20$ and are accurate to 3 digits.

3.2. *Numerical and asymptotic results for the permeability function $g(q)$*

Results for the permeability function $g(q)$ are shown graphically in figure 2 and provided in tabular form in the Supplementary Material. The limiting behaviours for small and large q, derived in Appendix B, are

$$g(q) = -\tfrac{12}{5}\log q + b_1 + b_2 q + O(q^2), \quad q \ll 1, \tag{3.17}$$

with $b_1 \doteq -0.48$ and $b_2 \doteq -1.5$, and

$$g(q) = c_1 q^{-5/2} + O\left(q^{-5}\right), \quad q \gg 1, \tag{3.18}$$

with $c_1 \doteq 2.12$. The results show that $g(q) > 0$, indicating that permeability reduces the lubrication pressure between particles undergoing transverse near-contact motion, i.e. $\hat{P}_\infty > \hat{P}$ according to (3.13).

4. Lubrication resistance functions for permeable spheres

We present here the complete set of resistance functions for near-contact motion of permeable particles, and discuss the effect of permeability.

4.1. *Transverse resistance functions*

Rearranging (2.23)–(2.28) to isolate the type of motion yields the forces, torques and stresslets in terms of resistance functions. The notation and general definition of resistance
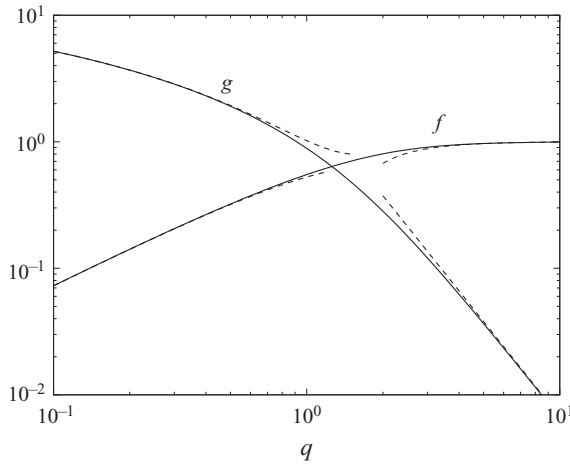
938 A27-10

Figure 2. Transverse and axisymmetric permeability functions $g(q)$ and $f(q)$, defined by (3.13) and (D5), respectively; numerical solutions (solid lines), asymptotic forms (3.17)–(3.18) and (D6)–(D7) (dashed lines). Tables of numerical values for $f(q)$ and $g(q)$ are provided in the Supplementary Material.

functions used in the literature is followed (Jeffrey 1992; Kim & Karrila 2005). The results are

$$-\frac{F_{x_1}}{\pi\mu U_0 a_1} = 6Y_{11}^A \bar{U}_1 + 4Y_{11}^B \bar{\omega}_1, \tag{4.1}$$

$$-\frac{F_{x_2}}{\pi\mu U_0 a_1} = 3(1+\kappa)Y_{21}^A \bar{U}_1 + (1+\kappa)^2 Y_{21}^B \bar{\omega}_1, \tag{4.2}$$

$$-\frac{T_{y_1}}{\pi\mu U_0 a_1^2} = 4Y_{11}^B \bar{U}_1 + 8Y_{11}^C \bar{\omega}_1, \tag{4.3}$$

$$-\frac{T_{y_2}}{\pi\mu U_0 a_1^2} = (1+\kappa)^2 Y_{21}^B \bar{U}_1 + (1+\kappa)^3 Y_{21}^C \bar{\omega}_1, \tag{4.4}$$

$$-\frac{S_{xz,1}}{\pi\mu U_0 a_1^2} = -4Y_{11}^G \bar{U}_1 + 8Y_{11}^H \bar{\omega}_1, \tag{4.5}$$

and

$$-\frac{S_{xz,2}}{\pi\mu U_0 a_1^2} = -(1+\kappa)^2 Y_{21}^G \bar{U}_1 + (1+\kappa)^3 Y_{21}^H \bar{\omega}_1. \tag{4.6}$$

Here, $Y_{\alpha\beta}^R(\xi, \kappa, q)$ are the transverse resistance functions, where the superscript R refers to one of the resistance tensors A, B, C, G or H in the resistance matrix (C1), and subscripts α and β refer to the particle labels 1 or 2. Using symmetry relations and the Lorentz reciprocal theorem, the grand resistance matrix can be derived from this set of resistance functions, as shown in Appendix C.

The transverse resistance functions are

$$Y_{\alpha\beta}^R(\xi, \kappa, q) = Y_{\alpha\beta}^{R,0}(\xi, \kappa) - g(q)\Upsilon_{\alpha\beta}^R(\kappa) + O\left(\xi \log \xi^{-1}\right), \tag{4.7}$$

where $Y_{\alpha\beta}^{R,0}$ are the hard-sphere resistance functions (C5)–(C14), $g(q)$ is the transverse permeability function (3.13) shown in figure 2 and $\Upsilon_{\alpha\beta}^R$ are the size-ratio-dependent

coefficients given by

$$\Upsilon_{11}^A = \frac{\kappa}{12}\frac{(1-\kappa)^2}{(\kappa+1)^3}, \quad \Upsilon_{21}^A = -\frac{\kappa}{6}\frac{(1-\kappa)^2}{(\kappa+1)^4}, \tag{4.8a,b}$$

$$\Upsilon_{11}^B = -\frac{\kappa}{8}\frac{(1-\kappa)}{(\kappa+1)^2}, \quad \Upsilon_{21}^B = \frac{\kappa^2}{2}\frac{1-\kappa}{(\kappa+1)^4}, \tag{4.9a,b}$$

$$\Upsilon_{11}^C = \frac{\kappa}{16(1+\kappa)}, \quad \Upsilon_{21}^C = -\frac{\kappa^2}{2(1+\kappa)^4}, \tag{4.10a,b}$$

$$\Upsilon_{11}^G = -\frac{(3\kappa-1)(1-\kappa)\kappa}{16(1+\kappa)^3}, \quad \Upsilon_{21}^G = \frac{(3-\kappa)(1-\kappa)\kappa^2}{4(1+\kappa)^5}, \tag{4.11a,b}$$

$$\Upsilon_{11}^H = -\frac{\kappa}{32}\frac{3\kappa-1}{(1+\kappa)^2}, \quad \Upsilon_{21}^H = \frac{\kappa^2}{4}\frac{3-\kappa}{(1+\kappa)^5}. \tag{4.12a,b}$$

Recall that $\xi = h_0/\bar{a}$ is the gap normalized by the average radius, $\kappa = a_2/a_1$ is the size ratio and $q = K^{-2/5}h_0/a$ is the permeability parameter. The result (4.7) indicates that particle permeability additively affects the transverse resistance functions.

4.2. *Axisymmetric resistance functions*

The leading-order axisymmetric resistance functions are presented here using the results of our recent analysis (Reboucas & Loewenberg 2021*a*). Following the presentation in § 4.1, the forces, torques and stresslets are (Jeffrey 1992; Kim & Karrila 2005)

$$-\frac{F_{z_1}}{\pi\mu U_0 a_1} = 6X_{11}^A \bar{U}_1, \quad -\frac{F_{z_2}}{\pi\mu U_0 a_1} = 3(1+\kappa)X_{21}^A \bar{U}_1, \tag{4.13a,b}$$

$$-\frac{T_{z_1}}{\pi\mu U_0 a_1^2} = 8X_{11}^C \bar{\omega}_1, \quad -\frac{T_{z_2}}{\pi\mu U_0 a_1^2} = (1+\kappa)^3 X_{21}^C \bar{\omega}_1, \tag{4.14a,b}$$

$$-\frac{S_{zz,1}}{\pi\mu U_0 a_1^2} = -4X_{11}^G \bar{U}_1, \quad -\frac{S_{zz,2}}{\pi\mu U_0 a_1^2} = -(1+\kappa)^2 X_{21}^G \bar{U}_1, \tag{4.15a,b}$$

where $\bar{U}_1$ and $\bar{\omega}_1$ are translational and rotational velocities of particle 1 along the line of centres, in the z-direction. Here, $X_{\alpha\beta}^R(\xi, \kappa, q)$ are the axisymmetric resistance functions, the superscript R refers to the resistance tensor A, C or G and subscripts α and β are particle labels 1 or 2. The remaining resistance functions for the grand resistance matrix (C1) for axisymmetric motion are derived from this set of functions, as shown in Appendix C.

The leading-order, axisymmetric resistance functions are

$$X_{\alpha\beta}^A(\xi, \kappa, q) = X_{\alpha\beta}^{A,0}(\xi, \kappa)f(q), \quad X_{\alpha\beta}^G(\xi, \kappa, q) = X_{\alpha\beta}^{G,0}(\xi, \kappa)f(q), \tag{4.16a,b}$$

where $X_{\alpha\beta}^{A,0}$ and $X_{\alpha\beta}^{G,0}$ are the hard-sphere resistance functions (C15)–(C18), and $f(q)$ is the axisymmetric permeability function (D5) shown in figure 2. This function was recently analysed (Reboucas & Loewenberg 2021*a*), and its primary features are summarized in Appendix D.

Particle permeability is seen to have a multiplicative effect on the axisymmetric resistance functions, in contrast to its additive effect on the transverse functions. Axisymmetric rotation does not generate a lubrication pressure thus, $X_{\alpha\beta}^C(\xi, \kappa, q) = X_{\alpha\beta}^{C,0}(\xi, \kappa)$.

938 A27-12

4.3. *Matching to the outer region*

Away from the near-contact region, hard-sphere resistance functions describe pairwise hydrodynamic interactions for permeable spheres to $O(K)$. According to (3.18) and (4.7) and (D7) and (4.16*a,b*), the resistance functions for permeable spheres presented in §4.1–4.2 are equal to the corresponding hard-sphere functions in the overlapping region

$$K^{2/5} \ll \epsilon \ll 1, \tag{4.17}$$

for $K \to 0$, where $\epsilon = h_0/a$ is the gap normalized by the reduced radius $a = a_1 a_2/(a_1 + a_2)$. Accordingly, the resistance functions for permeable spheres match asymptotically to the hard-sphere functions. This provides a uniformly valid approximation for the resistance functions

$$Z_{\alpha\beta}^R(\xi, \kappa, q) = Z_{\alpha\beta}^{R,0}(\xi, \kappa) + Z_{L\alpha\beta}^R(\xi, \kappa, q) - Z_{L\alpha\beta}^{R,0}(\xi, \kappa), \tag{4.18}$$

where $Z_{\alpha\beta}^R$ is a pairwise resistance function for permeable spheres, $Z_{\alpha\beta}^{R,0}$ is the corresponding hard-sphere resistance function, $Z_{L\alpha\beta}^{R,0}$ is the lubrication approximation for the hard-sphere function and $Z_{L\alpha\beta}^R$ is the lubrication resistance function for permeable spheres, as developed in our study.

4.4. *Non-singular particle motions*

The qualitative effects of particle permeability on the lubrication resistances are discussed below. Permeability relieves the lubrication pressure in the near-contact region, as discussed at the end of §3.2 and at the end of Appendix D. We show here that permeability qualitatively alters near-contact motion of particles and gives rise to additional non-singular contact motions that are inaccessible to hard spheres. For hard spheres, only rigid-body motions, i.e. pair translation and dumbbell rotation, and relative rotations about the symmetry axis are non-singular at contact. As a result of permeability, non-shearing motions of particles in contact also become non-singular. These include rolling without slip and axisymmetric approach.

4.4.1. *Transverse motions*

Particle permeability lessens the magnitude of the transverse lubrication function $Y_{\alpha\beta}^R$ if the contributions $Y_{\alpha\beta}^{R,0}$, $\Upsilon_{\alpha\beta}^R$ in (4.7) have the same algebraic sign; the latter is determined by formulas (4.8*a,b*)–(4.10*a,b*) and (C5)–(C10). It is thus seen that permeable particles of unequal size have lower translational resistances, Y_{11}^A, Y_{21}^A; translational resistances for equal-size particles are unaffected by permeability. Permeability reduces the rotational resistance Y_{11}^C of a particle spinning close to a stationary particle but it enhances the rotational coupling between the particles, increasing Y_{21}^C.

To generally explain the role of permeability in transverse particle motions, it is convenient to examine the forces, torques and stresslets given by (2.23)–(2.28). The effect of permeability depends on whether the contribution from the lubrication pressure, $I_1 - I_K$, reinforces or opposes the contribution from shearing motion of the particle surfaces, I_2; permeability reduces the magnitude of the former contribution, but has no effect on the latter. Accordingly, the net effect of particle permeability depends on the coefficients of $I_1 - I_K$ and I_2 in (2.23)–(2.28).

The forces, torques and stresslets for the special case of particle motion prescribed by

$$(\kappa - 1)\bar{U}_1 + (\kappa + 1)\bar{\omega}_1 = 0, \quad \bar{U}_2 = \bar{\omega}_2 = 0 \qquad (4.19a,b)$$

are unaffected by particle permeability because $C = 0$ in this case, according to (2.15), and thus the pressure contribution, associated with $I_1 - I_K$, vanishes in (2.23)–(2.28). This result explains why the translational resistances for equal-size particles are unaffected by permeability.

Conversely, the shearing contribution vanishes in (2.23)–(2.28) for rolling motion of the particles without slip,

$$\bar{U}_1 = \bar{\omega}_1 = 1, \quad \bar{U}_2 = \bar{\omega}_2 = 0, \qquad (4.20a,b)$$

because $B = 0$, according to (2.29). The forces, torques, and stresslets in this case are due entirely to the pressure contribution $I_1 - I_K$, and thus have reduced magnitudes for permeable particles. Moreover, rolling motion of permeable particles is non-singular at contact, as shown by combining (3.1), (3.17) and (C4a) to yield,

$$\lim_{\xi \to 0} (I_1 - I_K) = \frac{24}{25}\left(1 + \kappa^{-1}\right)^{-2} \log K^{-1} + C_0, \qquad (4.21)$$

where C_0 depends only on size ratio. Other rolling motions without slip (e.g. pure rotation; $-\kappa\bar{\omega}_2 = \bar{\omega}_1 = 1$, $\bar{U}_1 = \bar{U}_2 = 0$) are also non-singular, and can be generated by a superposition of (4.20a,b) with non-singular rigid-body translation and rotation.

4.4.2. *Axisymmetric motions*

Given the form of the axisymmetric resistances (C15)–(C18), and formula (D6), it follows that axisymmetric resistances (4.16a,b) have the limiting forms,

$$\lim_{\xi \to 0} X_{\alpha\beta}^A(\xi, \kappa, q) = \chi_{\alpha\beta}^A(\kappa)K^{-2/5}, \quad \lim_{\xi \to 0} X_{\alpha\beta}^G(\xi, \kappa, q) = \chi_{\alpha\beta}^G(\kappa)K^{-2/5}, \qquad (4.22a,b)$$

where the functions $\chi_{\alpha\beta}^A(\kappa)$ and $\chi_{\alpha\beta}^G(\kappa)$ depend only on the size ratio. The result demonstrates that the axisymmetric resistances for permeable particles are non-singular at contact in contrast to the ξ^{-1} singular resistances for hard spheres.

5. Mobility functions

Here, we present pairwise mobilities of permeable particles defined by the relative velocity of the particles $U_{12} = U_2 - U_1$ under the actions of forces and an imposed flow (Batchelor & Green 1972; Batchelor 1982)

$$
\begin{aligned}
U_{12} = {} & \left[G(s)\hat{r}\hat{r} + H(s)\left(I - \hat{r}\hat{r}\right)\right] \cdot U_{12,0}^{\infty} \\
& + \left[L(s)\hat{r}\hat{r} + M(s)\left(I - \hat{r}\hat{r}\right)\right] \cdot U_{12,g}^{\infty} \\
& + E_\infty \cdot r + \omega_\infty \times r - \left[A(s)\hat{r}\hat{r} + B(s)\left(I - \hat{r}\hat{r}\right)\right] \cdot E_\infty \cdot r. \qquad (5.1)
\end{aligned}
$$

Here, $r = x_2 - x_1$ is the vector between the particle centres, $\hat{r} = r/|r|$ is a unit vector along the line of centres, I is the identity tensor and $s = |r|/\bar{a}$ is the centre-to-centre separation normalized by the average radius, $\bar{a} = \frac{1}{2}(a_1 + a_2)$. The quantities E_∞ and ω_∞ are the imposed rate of strain and vorticity in the fluid, and $U_{12,0}^{\infty}$ and $U_{12,g}^{\infty}$ are, respectively,

the relative velocities in the absence of hydrodynamic interactions (i.e. $s \to \infty$) under the action of equal and opposite forces and under the action of gravity

$$U_{12,0}^{\infty} = \frac{F_2 - F_1}{6\pi\mu a}, \quad U_{12,g}^{\infty} = \frac{2\left(a_2^2\gamma - a_1^2\right)\Delta\rho_1 g}{9\mu}, \tag{5.2a,b}$$

where $F_1 = -F_2$, a is the reduced radius, g is the acceleration due to gravity, $\Delta\rho_i = \rho_i - \rho$ is the difference between the density of particle i ($i = 1, 2$) and the density of the fluid and

$$\gamma = \frac{\Delta\rho_2}{\Delta\rho_1}, \tag{5.3}$$

is the ratio of particle density differences.

Equation (5.1) defines the pairwise axisymmetric and transverse mobility functions G, L, A and H, M, B, respectively. According to their definitions, G, H, L and M tend to unity at large separations, whereas A and B vanish for $s \to \infty$. The pair mobilities depend on the centre-to-centre separation, s, size ratio, κ, and permeability, K (L and M also depend on the density difference ratio, γ). For the weak permeability regime (1.2) considered herein, hard-sphere mobilities can be used outside of the near-contact region with $O(K)$ error.

The near-contact mobilities H, M, B for transverse motion were obtained by inverting the resistance matrix (C1). The near-contact axisymmetric mobility G was similarly obtained, and mobilities L and A derived by an analysis of the contact forces between spheres migrating along their line of centres, as described in section § 5.2. Outside of the near-contact region, mobilities were calculated using a code based on a bispherical coordinate solution for hard spheres provided by A.Z. Zinchenko.

5.1. *Transverse mobilities*

The transverse mobilities H, M and B have the near-contact form

$$\Lambda(\xi, \kappa, K) = \frac{\lambda_1 + \lambda_2 \log\xi^{-1} + \lambda_3 \left[\log\xi^{-1} - \frac{5}{12}g(q)\right]\log\xi^{-1} + \lambda_6 g(q)}{\lambda_4 + \lambda_5 \log\xi^{-1} + \left[\log\xi^{-1} - \frac{5}{12}g(q)\right]\log\xi^{-1} + \lambda_7 g(q)}, \tag{5.4}$$

where $\xi = h_0/\bar{a}$ is the gap normalized by the average radius, and $q = K^{-2/5}h_0/a$ is the permeability parameter. The coefficients λ_i ($i = 1$–7) depend only on the size ratio; numerical values for several size ratios are listed in tables 1–3.

The results shown in figures 3–5 demonstrate that permeability quantitatively affects the transverse mobilities for $\xi \lesssim O(K^{2/5})$, corresponding to $q = O(1)$, and has the largest effect for extreme size ratios. Particle permeability has no effect for equal-size particles, as seen in figures 3 and 5, because no lubrication pressure is generated by the motion, as discussed in § 4.4.1.

Figures 3–4 show that mobility functions H and M for permeable particles are larger than for hard spheres, whereas the opposite is true for mobility function B, as shown in figure 5. These observations indicate that particle permeability diminishes the strength of hydrodynamic pair interactions in all cases, given that $H = M = 1$ and $B = 0$ in the absence of hydrodynamic interactions.

κ	λ_1	λ_2	λ_3	λ_4	λ_5	λ_6	λ_7
1	5.087	2.967	0.4010	6.325	6.043	−0.4514	−0.5613
0.9	5.066	2.969	0.3997	6.272	6.036	−0.4514	−0.5589
0.75	4.921	2.980	0.3911	5.927	5.985	−0.4508	−0.5428
0.6	4.555	2.995	0.3696	5.105	5.831	−0.4479	−0.5020
0.5	4.100	2.993	0.3432	4.177	5.599	−0.4425	−0.4509
0.4	3.387	2.956	0.3027	2.877	5.163	−0.4313	−0.3686
0.3	2.317	2.849	0.2443	1.222	4.378	−0.4103	−0.2378
0.25	1.623	2.756	0.2080	0.3221	3.796	−0.3951	−0.1465
0.125	−0.6696	2.393	0.1033	−1.540	1.516	−0.3451	0.2069

Table 1. Coefficients of transverse mobility H given by (5.4).

κ	λ_1	λ_2	λ_3	λ_4	λ_5	λ_6	λ_7
0.9	3.128	2.1402	0.2206	6.272	6.036	−0.2745	−0.5589
0.75	2.942	2.104	0.2075	5.926	5.985	−0.2661	−0.5428
0.6	2.529	2.022	0.1794	5.105	5.831	−0.2477	−0.5020
0.5	2.074	1.915	0.1497	4.177	5.599	−0.2267	−0.4509
0.4	1.461	1.736	0.1114	2.877	5.163	−0.1965	−0.3686
0.3	0.7212	1.461	0.06812	1.222	4.378	−0.1560	−0.2378
0.25	0.3448	1.276	0.04718	0.3221	3.796	−0.1326	−0.1465
0.125	−0.3928	0.6909	9.123×10^{-3}	−1.540	1.516	−0.06637	0.2069

Table 2. Coefficients of transverse mobility M ($\gamma = 1$) given by (5.4).

κ	λ_1	λ_2	λ_3	λ_4	λ_5	λ_6	λ_7
1	−1.902	1.501	0.4060	6.325	6.043	0.1688	−0.5613
0.9	−1.894	1.496	0.4106	6.272	6.036	0.1686	−0.5589
0.75	−1.842	1.465	0.4403	5.926	5.985	0.1681	−0.5428
0.6	−1.716	1.378	0.5089	5.105	5.831	0.1682	−0.5020
0.5	−1.566	1.262	0.5831	4.177	5.599	0.1711	−0.4509
0.4	−1.348	1.063	0.6822	2.877	5.163	0.1816	−0.3686
0.3	−1.059	0.7307	0.7987	1.222	4.378	0.2112	−0.2378
0.25	−0.8967	0.4932	0.8572	0.3231	3.796	0.2403	−0.1465
0.125	−0.5606	−0.4511	0.9707	−1.540	1.516	0.4213	0.2069

Table 3. Coefficients of transverse mobility B given by (5.4).

Inserting (3.17) into (5.4) and taking the limit as $\xi \to 0$ yields the contact values of the transverse mobilities

$$\Lambda_c(\kappa, K) = \lambda_3 \frac{\log K^{-1} + \lambda_1'}{\log K^{-1} + \lambda_2'}, \quad \xi = 0, \tag{5.5}$$

where Λ_c is the contact value of the transverse mobility function H, M or B, and the coefficients λ_1' and λ_2' are given by

$$\lambda_1' = 6\lambda_6\lambda_3^{-1} + \tfrac{5}{2}\lambda_2\lambda_3^{-1} - \tfrac{5}{2}\log v - \tfrac{25}{24}b_1, \tag{5.6a}$$

$$\lambda_2' = 6\lambda_7 + \tfrac{5}{2}\lambda_5 - \tfrac{5}{2}\log v - \tfrac{25}{24}b_1, \tag{5.6b}$$
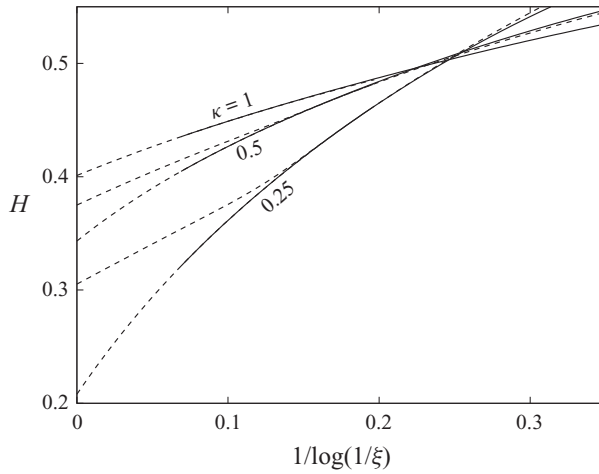
Figure 3. Transverse mobility functions H from exact solution for hard spheres using code from A. Z. Zinchenko (solid lines) and lubrication solutions for hard spheres, $K = 0$, and permeable spheres, $K = 10^{-7}$ (dashed lines) vs gap, ξ, for size ratios indicated. Lubrication solution for hard spheres appears as a continuation of the exact solution; the lubrication solution for permeable spheres deviates for $\xi \lesssim K^{2/5}$.
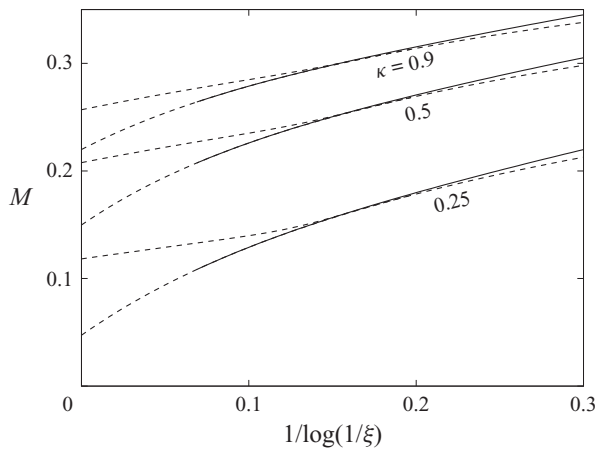

Figure 4. Same as figure 3, except for the transverse mobility function M.

where $\nu = 2\kappa(1 + \kappa)^{-2}$ and $b_1 \doteq -0.48$. For convenience, values for λ'_1 and λ'_2 are listed in table 4. Contact values for the mobilities of hard spheres are given by λ_3; even small permeabilities can significantly alter contact mobilities because its effect decays only logarithmically.

According to formula (5.5), Λ_c increases with K for $\lambda'_1 > \lambda'_2$, decreases for $\lambda'_1 < \lambda'_2$, the effect is largest for disparate values of these parameters, and Λ_c is independent of K for $\lambda'_1 = \lambda'_2$. Consistent with the discussion above and the results shown in figures 3–5, the values in table 4 thus indicate that contact values of mobilities H and M increase with K, B decreases with K, the effect is largest for extreme size ratios and Λ_c is independent of K for equal-size particles.
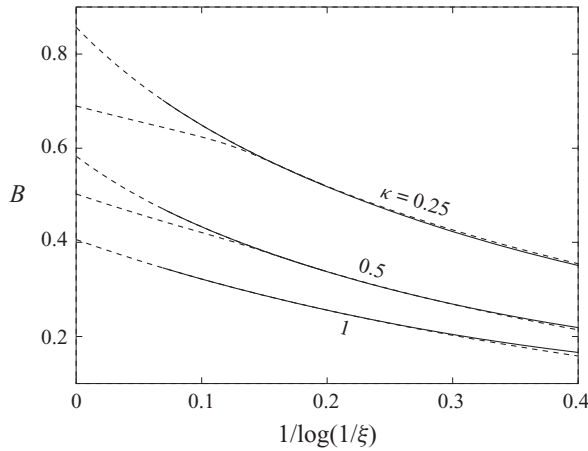
938 A27-17

Figure 5. Same as figure 3, except for the transverse mobility function B.

κ	H		M ($\gamma = 1$)		B	
	λ'_1	λ'_2	λ'_1	λ'_2	λ'_1	λ'_2
1	0	0	—	—	0	0
0.9	14.03	13.98	19.03	13.98	13.81	13.98
0.75	14.42	13.99	19.94	13.99	12.89	13.99
0.6	15.39	13.96	22.29	13.96	12.33	13.85
0.5	16.59	13.82	25.43	13.82	9.697	13.82
0.4	18.60	13.44	31.18	13.44	8.232	13.44
0.3	22.17	12.61	42.98	12.61	6.963	12.61
0.25	25.08	11.96	54.09	11.96	6.471	11.96
0.125	42.42	9.585	150.3	9.585	5.997	9.585

Table 4. Coefficients for the contact values of transverse mobilities given by (5.5).

5.2. *Axisymmetric mobilities*

The axisymmetric mobility G has the near-contact form

$$G = \frac{(1+\kappa)^2}{2\kappa} \frac{\xi}{f(q)} = \frac{\epsilon}{f(q)}, \quad \xi \ll 1, \tag{5.7}$$

where $\xi = h_0/\bar{a}$ and $\epsilon = h_0/a$ are the gaps normalized by the average and reduced radius, respectively, κ is the size ratio and $q = K^{-2/5} h_0/a$ is the permeability parameter. Inserting (D6)–(D7) into (5.7) yields

$$G = \left(b_0 + b_1 q + O(q^2)\right) K^{2/5}, \quad q \ll 1, \tag{5.8}$$

and

$$G = \left(1 + c_0 q^{-5/2} + O(q^{-5})\right) \epsilon, \quad q \gg 1, \tag{5.9}$$

where $b_0 \doteq 1.332$, $b_1 \doteq 0.397$ and $c_0 \doteq 1.8402$. The result for hard spheres is recovered from the latter for $q \to \infty$. Equation (5.8) indicates that the particles undergo a constant approach velocity at contact under the action of a constant force, consistent with the non-singular axisymmetric resistances for permeable particles given by (4.22a,b).
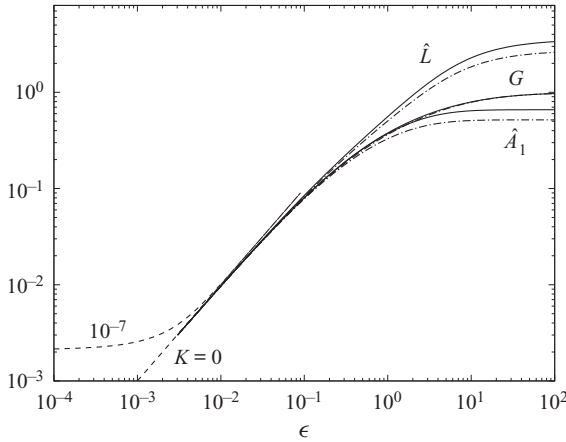
938 A27-18

Figure 6. Axisymmetric mobility functions $\hat{A}_1$ and $\hat{L}$ ($\gamma = 1$), defined by (5.10*a,b*), and G for hard spheres vs gap, $\epsilon = h_0/a$, for size ratios $\kappa = 0.5$ (solid lines), and $\kappa = 0.75$ (dash-dotted lines) using code from A. Z. Zinchenko (curves for $\kappa = 0.5$, and $\kappa = 0.75$ are indistinguishable for G); lubrication solution for hard spheres, $K = 0$, and permeable spheres $K = 10^{-7}$ (dashed lines).

In the near-contact region, L and $1 - A$ are proportional to G, motivating the definition of modified mobility functions $\hat{L}$ and $\hat{A}_1$

$$\hat{L}(\epsilon, \kappa, q) = \frac{L(\epsilon, \kappa, q)}{\hat{F}_c^{(g)}(\kappa)}, \quad \hat{A}_1(\epsilon, \kappa, q) = \frac{1 - A(\epsilon, \kappa, q)}{\hat{F}_c^{(E)}(\kappa)}, \quad (5.10a,b)$$

with the property

$$\lim_{\epsilon \to 0} \hat{L}(\epsilon, \kappa, q) = \lim_{\epsilon \to 0} \hat{A}_1(\epsilon, \kappa, q) = \lim_{\epsilon \to 0} G(\epsilon, q), \quad (5.11)$$

where $\hat{F}_c^{(g)}$ and $\hat{F}_c^{(E)}$ are dimensionless contact forces, obtained by the procedure described in Appendix E and given by (E3)–(E4). These forces arise between two spheres in point contact, migrating along their line of centres in gravity-driven motion, and in axisymmetric straining flow, respectively. The mobility function L also depends on the ratio of the particle density differences, γ, defined by (5.3). Numerical values of the contact forces are provided in table 6 for several size ratios.

Axisymmetric mobilities $G, \hat{L}$ and $\hat{A}_1$ are shown in figure 6 as a function of gap where the common behaviour of the modified axisymmetric mobilities (5.11) is demonstrated; permeability qualitatively changes the near-contact motion for $h_0/a \leq O(K^{2/5})$, corresponding to $q \leq O(1)$. Figure 7 shows the universal near-contact behaviour predicted by combining (5.7) and (5.11)

$$GK^{-2/5} = \hat{A}_1 K^{-2/5} = \hat{L}K^{-2/5} = \frac{q}{f(q)}, \quad \epsilon \to 0. \quad (5.12)$$

5.3. *Mobility of a particle moving parallel to a wall*

In this section, the motion of a sphere in close contact with a wall is considered, corresponding to the limit $\kappa \to \infty$. Two problems are studied: (I) motion of a particle in a quiescent fluid under the action of an imposed force $F = F_0 e_x$ parallel to the wall and (II)
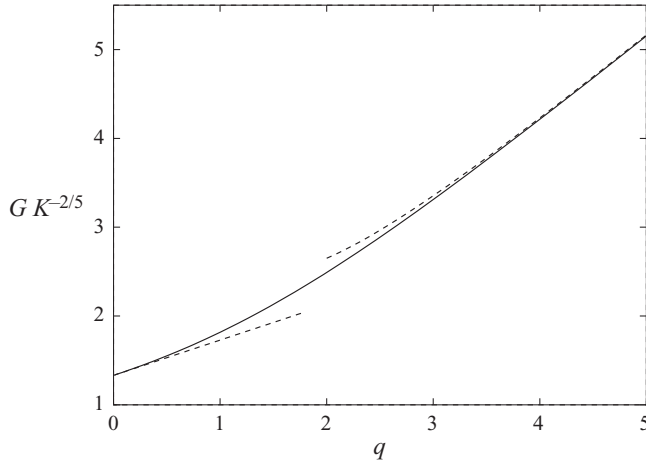
Figure 7. Universal near-contact behaviour (5.12) vs permeability parameter, q (solid line); small- and large-q asymptotes given by (5.8)–(5.9) (dashed lines).

motion of a force-free particle in an imposed shear flow parallel to the wall, $U_\infty = E_\infty z e_x$. The particle is torque free in both problems.

The resistance formulation for problems (I) and (II), derived from the general resistance formulation (C1) for the particle–wall configuration ($\kappa \to \infty$), is

$$-\frac{F_{x_1}}{\pi \mu U_0 a_1} = 6Y_{11}^{A,\infty} \bar{U}_1 + 4Y_{11}^{B,\infty} \bar{\omega}_1 - (6Y_{11}^{A,\infty} + 2Y_{11}^{B,\infty} - 4Y_{11}^{G,\infty})\bar{E}_\infty, \quad (5.13)$$

$$-\frac{T_{y_1}}{\pi \mu U_0 a_1^2} = 4Y_{11}^{B,\infty} \bar{U}_1 + 8Y_{11}^{C,\infty} \bar{\omega}_1 - (4Y_{11}^{B,\infty} + 4Y_{11}^{C,\infty} + 8Y_{11}^{H,\infty})\bar{E}_\infty, \quad (5.14)$$

where a_1 is the radius of the sphere, $\bar{U}_1 = U_1/U_0$ and $\bar{\omega}_1 = \omega_1 a_1/U_0$ are the dimensionless translational and rotational velocities, $\bar{E}_\infty = E_\infty a_1/U_0$ is the dimensionless shear rate and $Y_{11}^{R,\infty}$ are the resistance functions (4.7) corresponding to the limit $\kappa \to \infty$

$$Y_{11}^{A,\infty} = -\frac{g(q)}{12} + \frac{8}{15}\log \epsilon^{-1} + A_{11}^{Y,\infty} + O(\epsilon \log \epsilon^{-1}), \quad (5.15)$$

$$Y_{11}^{B,\infty} = -\frac{g(q)}{8} - \frac{1}{5}\log \epsilon^{-1} + B_{11}^{Y,\infty} + O(\epsilon \log \epsilon^{-1}), \quad (5.16)$$

$$Y_{11}^{C,\infty} = -\frac{g(q)}{16} + \frac{2}{5}\log \epsilon^{-1} + C_{11}^{Y,\infty} + O(\epsilon \log \epsilon^{-1}). \quad (5.17)$$

$$Y_{11}^{G,\infty} = -\frac{3}{16}g(q) + \frac{7}{10}\log \epsilon^{-1} + G_{11}^{Y,\infty} + O(\epsilon \log \epsilon^{-1}). \quad (5.18)$$

$$Y_{11}^{H,\infty} = \frac{3}{32}g(q) - \frac{1}{10}\log \epsilon^{-1} + H_{11}^{Y,\infty} + O(\epsilon \log \epsilon^{-1}). \quad (5.19)$$

Here, $\epsilon = h_0/a_1$ is the dimensionless gap, $q = K^{-2/5}h_0/a_1$ is the permeability parameter, $g(q)$ is the transverse mobility function and $R_{11}^{Y,\infty}$ are the matching constants to the outer solution for this geometry (Goldman *et al.* 1967*a*,*b*; Corless & Jeffrey 1988*b*).

938 A27-20

	$\bar{U}_1$					
Problem	λ_0	λ_1	λ_2	λ_3	λ_4	λ_5
(I)	1.909	2.000	-0.3125	1.590	3.1881	-0.3008
(II)	2.649	3.716	-0.3348	1.590	3.1881	-0.3008
	$\bar{\omega}_1$					
	λ_0	λ_1	λ_2	λ_3	λ_4	λ_5
(I)	-0.9475	0.5000	0.3125	1.590	3.1881	-0.3008
(II)	0.6513	2.109	0.3348	1.590	3.1881	-0.3008

Table 5. Coefficients for particle velocity parallel to wall (5.20).
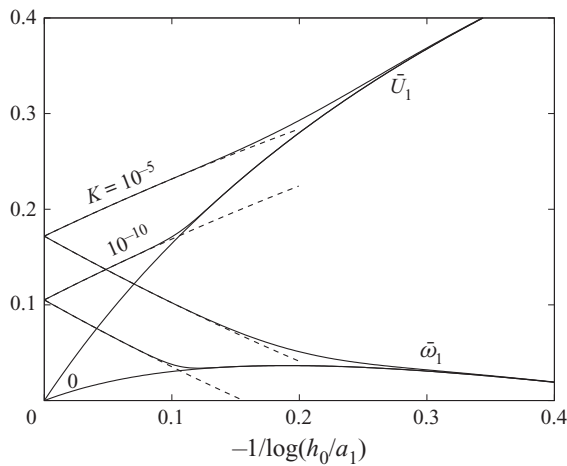
Figure 8. Translational and rotational velocities of a particle moving parallel to a plane wall under the action of a force; mobility formula (5.20) (solid lines); simplified mobility formula for $q \ll 1$ obtained by inserting (3.17) into (5.20) (dashed lines); permeabilities as labelled.

The translational and rotational mobilities of the particle are determined by solving (5.13) and (5.14), separately, for problems (I) and (II). The results are

$$\bar{V}_1 = \frac{\lambda_0 + \lambda_1 \log \epsilon^{-1} + \lambda_2 g(q)}{\lambda_3 + \lambda_4 \log \epsilon^{-1} + \left[\log \epsilon^{-1} - \frac{5}{12} g(q) \right] \log \epsilon^{-1} + \lambda_5 g(q)}, \tag{5.20}$$

where $\bar{V}_1 = \bar{U}_1$ or $\bar{V}_1 = \bar{\omega}_1$, and $U_0 = (6\pi\mu a_1)^{-1} F_0$ for problem (I), and $U_0 = E_\infty a_1$ for problem (II). The numerical coefficients appearing in (5.20) are listed in table 5 for both problems, and the results are plotted in figures 8 and 9. The results for hard spheres (Goldman *et al.* 1967*a*,*b*; Corless & Jeffrey 1988*b*) are recovered for $g = 0$, corresponding to $q \to \infty$.

Inserting (3.17) into (5.20) yields a simplified analytical mobility formula depicted by the dashed lines in figures 8–9. Evaluating the result at contact yields

$$\bar{U}_1 = \bar{\omega}_1 = \frac{d_1}{\log K^{-1} + d_2}, \tag{5.21}$$
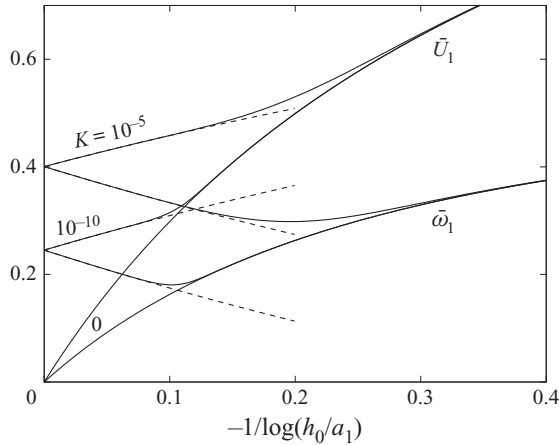
Figure 9. Same as 8, except for a particle moving parallel to a plane wall in shear flow.

indicating that permeable particles roll without slipping. Here, $d_1 = 3.125$, $d_1 = 7.280$ for problems (I), (II), respectively, and $d_2 = 6.666$ for both problems. This finding illustrates the non-singular rolling motion accessible to permeable particles at contact, as discussed in § 4.4. Hard spheres, by contrast, become stationary at contact and exhibit a slipping approach to contact with $\bar{U}_1 > \bar{\omega}_1$ (Goldman *et al.* 1967*a*,*b*), as seen in figures 8–9.

6. Conclusions

A lubrication analysis is presented for permeable, spherical particles using Darcy's law to describe the intraparticle velocity. Only the mean permeability enters the problem and the size ratio is arbitrary. The complete resistance matrix is derived for near-contact motions.

Under the weak permeability conditions (1.2) considered herein, particle permeability enters only in the lubrication regime, where it modifies the hydrodynamic resistances through the permeability functions, $f(q)$ and $g(q)$, describing particle motions along and perpendicular to the line of centres, respectively, and $q = (h_0/a)K^{-2/5}$ is the permeability parameter. The permeability functions are obtained by solving an integral form of the Reynolds lubrication equation that results from the non-local coupling between the pressure in the gap and the intraparticle pressure. Outside of the near-contact region, the resistance functions can be approximated by hard-sphere functions and the two are equal in a finite matching region. Particle permeability removes the contact singularity for all non-shearing particle motions, allowing contacting permeable particles to roll without slipping and touching particles to separate with finite velocity.

Axisymmetric mobilities have a universal near-contact behaviour that depends only on the permeability parameter q and attain non-vanishing values at contact, proportional to $K^{2/5}$. Permeability enhances transverse mobilities, especially for extreme size ratios, but has no effect on equal-size particles because the relative particle motion in this case does not generate a lubrication pressure. Under the action of a constant force, or an imposed shear flow, a permeable particle in point contact with a planar boundary rolls with an $O(1/\log K^{-1})$ velocity, according to a formula derived herein. The same formula also describes a hard sphere rolling on a permeable half-space which may have relevance to cross-flow particle filtration.

Author ORCIDs.
Rodrigo B. Reboucas https://orcid.org/0000-0001-8982-3553;
Michael Loewenberg https://orcid.org/0000-0003-1735-0755.

Appendix A. Derivation of intraparticle flux

In this appendix, we derive the combined intraparticle flux as a boundary integral of the pressure distribution in the near-contact region, given by formula (3.8) in the text. Unscaled, dimensional variables are used here. By Darcy's law (1.1) and the incompressibility of the fluid, the intraparticle pressure fields p_1 and p_2 satisfy Laplace's equation. The combined intraparticle flux is

$$2j = \frac{k_1}{\mu} \frac{\partial p_1}{\partial n} + \frac{k_2}{\mu} \frac{\partial p_2}{\partial n}, \tag{A1}$$

where pressure gradients are evaluated on the particle surfaces, and $\boldsymbol{n}$ is the outward normal vector. By continuity of pressure across the particle surfaces, the lateral lubrication length scale L and angular dependence (2.7a) of the pressure distribution in the lubrication gap are imposed on the intraparticle pressure fields.

There are two length scales that can determine the lateral length scale of the lubrication region, the geometrically imposed length L_0, given by equation (3.5), and L_K, a length scale set by the permeability (Reboucas & Loewenberg 2021a)

$$L_k = K^{1/5} a. \tag{A2}$$

In this appendix, L is the maximum of these two length scales

$$L = \max(L_0, L_k), \tag{A3}$$

and $L/a \ll 1$ is assumed, where a is the reduced radius.

As shown below, the intraparticle pressure fields decay to zero away from the near-contact region inside the particles on the length scale L. A semi-infinite permeable region can thus be considered given that $L/a \ll 1$. A cylindrical coordinate system (r, θ, z) is used, where $z < 0$ is the permeable region and $z > 0$ is the fluid region. This is shown in figure 10. Normal derivatives of pressure on the particle boundary can be approximated by a z-derivative with error $O(L/a)^2$. Moreover, the intraparticle pressure fields are the same in each particle because they are forced only by the pressure distributions on their surfaces in the near-contact region, which are the same because pressure variations across the gap are negligible according to the leading-order lubrication equations (2.1a–d). Accordingly, (A1) simplifies to

$$j = \frac{k}{\mu} \frac{\partial p_i}{\partial z} \bigg|_{z=0}, \tag{A4}$$

where p_i denotes the intraparticle pressure. The result indicates that the total intraparticle flux depends only on the mean permeability (1.3).
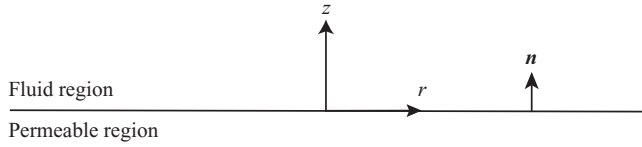
Figure 10. Cylindrical coordinate system and orientation of normal vector n used to describe pressure distribution in semi-infinite permeable region, $z < 0$.

As discussed above, the intraparticle pressure field has the angular dependence

$$p_i(r, \theta, z) = P_i(r, z) \cos \theta, \tag{A5}$$

imposed by continuity of the pressure at the particle–fluid interface, and it satisfies Laplace's equation. Hence, $P_i(r, z)$ satisfies

$$\frac{1}{r} \frac{\partial}{\partial r} \left[\frac{1}{r} \frac{\partial}{\partial r} (rP_i) \right] + \frac{\partial^2 P_i}{\partial z^2} = 0 \tag{A6}$$

in the semi-infinite region shown in figure 10, vanishes for $z \to -\infty$ and matches the pressure, $p(r, \theta)$, in the lubrication gap at $z = 0$.

A first-order Hankel transform of this equation with the prescribed boundary conditions yields

$$\frac{\mathrm{d}^2 Q_i}{\mathrm{d}z^2} - \omega^2 Q_i = 0; \quad Q_i(\omega, 0) = \int_0^\infty J_1(\omega r) P(r) r \, \mathrm{d}r, \quad Q_i(\omega, -\infty) = 0, \tag{A7a–c}$$

where $Q_i(\omega, z) = \int_0^\infty J_1(\omega r) P_i(r, z) r \, \mathrm{d}r$ is the Hankel-transformed intraparticle pressure, and $P(r)$ is the pressure in the lubrication gap. The solution of the transformed problem is

$$Q_i(\omega, z) = Q_i(\omega, 0) \, \mathrm{e}^{\omega z}, \tag{A8}$$

where $Q_i(\omega, 0)$ is the Hankel-transformed pressure distribution in the gap between the particles (A7b); by the inverse Hankel transform, the intraparticle pressure is given by

$$P_i(r, z) = \int_0^\infty Q_i(\omega, 0) \, \mathrm{e}^{\omega z} J_1(\omega r) \omega \, \mathrm{d}\omega. \tag{A9}$$

For $-z \gg 1$,

$$P_i(r, z) = \frac{3rzI}{(r^2 + z^2)^{5/2}}, \tag{A10}$$

which is obtained using $P(\omega, 0) \approx \omega I$ for $\omega L \ll 1$, where $I = \int_0^\infty P r^2 \, \mathrm{d}r$. This result confirms the decay of pressure away from the near-contact region.

From (A9), the normal derivative of pressure on the particle surface is

$$\left.\frac{\partial P_i}{\partial z}\right|_{z=0} = \int_0^\infty \omega^2 Q(\omega, 0) J_1(\omega r)\, d\omega. \tag{A11}$$

Rewriting this result using the identity

$$-\omega^2 Q(\omega, 0) = \int_0^\infty \frac{1}{r'}\frac{d}{dr'}\left[\frac{1}{r'}\frac{d}{dr'}\left[r' P(r', 0)\right]\right] J_1(\omega r') r'\, dr', \tag{A12}$$

yields

$$\left.\frac{\partial P_i}{\partial z}\right|_{z=0} = -\int_0^\infty \frac{1}{r'}\frac{d}{dr'}\left[\frac{1}{r'}\frac{d}{dr'}\left[r' P(r', 0)\right]\right] \phi\left(r'/r\right) dr', \tag{A13}$$

where

$$\phi\left(r'/r\right) = r' \int_0^\infty J_1(\omega r') J_1(\omega r)\, d\omega, \tag{A14}$$

and rewriting the Bessel function integral yields the Green's function,

$$\phi(x) = \frac{1}{\pi}\left[\frac{1+x^2}{1+x} K\left(\frac{2\sqrt{x}}{1+x}\right) - (1+x) E\left(\frac{2\sqrt{x}}{1+x}\right)\right], \tag{A15}$$

where $x = r'/r$, and K and E are elliptic integrals of the first and second kind

$$K(t) = \int_0^{\pi/2} \frac{d\theta}{\sqrt{1-t^2\sin^2\theta}}, \quad E(t) = \int_0^{\pi/2} \sqrt{1-t^2\sin^2\theta}\, d\theta. \tag{A16a,b}$$

The rescaled intraparticle flux (3.8) is obtained by recasting (A13) in terms of the dimensionless variables (3.4a–d).

A.1. *Properties of the Green's function*

The Green's function (A15) is seen to satisfy the reciprocal relation

$$\phi\left(1/x\right) = \frac{\phi(x)}{x}. \tag{A17}$$

A series expansion of (A15) for $x \ll 1$ yields

$$\phi(x) = \tfrac{1}{2}x^2 + \tfrac{3}{16}x^4 + O(x^6). \tag{A18}$$

Combining this result with the reciprocal relation (A17) gives

$$\phi(x) = \tfrac{1}{2}x^{-1} + \tfrac{3}{16}x^{-3} + O(x^{-5}) \tag{A19}$$

for $x \gg 1$. The Green's function has the log singular expansion at $x = 1$

$$\phi(x) = -\frac{1}{\pi}\left[\left(1 + \frac{1}{2}(x-1) - \frac{1}{16}(x-1)^2\right)\log\left(\frac{1}{8}|x-1|\right)\right.$$
$$\left. +2 + \frac{1}{2}(x-1) - \frac{3}{16}(x-1)^2\right]$$
$$+ O\left[(1-x)^3 \log|1-x|\right] + O(1-x)^3. \tag{A20}$$

938 A27-25

Appendix B. Analysis of transverse permeability function for large and small q

Here, the transverse permeability function $g(q)$ is analysed for the limits of small and large values of the parameter q.

B.1. *Small q limit*

The Reynolds equation (3.10) is singular for $q \to 0$ (i.e. $h_0 \to 0$) but a non-singular solution for $q = 0$ is possible by introducing dimensionless variables defined by the permeability length scale, L_k, rather than the geometric length scale, L_0. The parameter q can be written as a ratio of these scales

$$q = (L_0/L_k)^2, \tag{B1}$$

where L_0 and L_k are defined by (3.5) and (A2), respectively.

The singularity at $q = 0$ is removed by recasting the problem in terms of the dimensionless variables

$$\tilde{r} = \frac{r}{L_k}, \quad \tilde{z} = \frac{za}{L_k^2}, \quad \tilde{P} = \frac{pL_k^3}{\mu U_0 a^2}, \quad \tilde{J} = \frac{Ja}{U_0 L_k}. \tag{B2a–d}$$

In these variables, the Reynolds equation (3.10) becomes

$$\tfrac{1}{12}\tilde{w}\tilde{h}^3 + \tfrac{1}{4}\left(\tilde{I}_A\left[\tilde{w}\right] + \tilde{I}_B\left[\tilde{w}\right]\right)\tilde{h}^2\tilde{r} - 2\tilde{J}\left[\tilde{w}\right] = -\tfrac{1}{2}\tilde{r}, \tag{B3}$$

where

$$\tilde{w}(\tilde{r}) = \left[\frac{1}{\tilde{r}}\left(\tilde{r}\tilde{P}\right)'\right]', \tag{B4}$$

$$\tilde{I}_A\left[\tilde{w}\right] = -\frac{1}{2}\int_{\tilde{r}}^{\infty}\tilde{w}\,\mathrm{d}r, \quad \tilde{I}_B\left[\tilde{w}\right] = \frac{1}{2}\int_0^{\tilde{r}}\left(\frac{r}{\tilde{r}}\right)^2\tilde{w}\,\mathrm{d}r, \tag{B5a,b}$$

and the rescaled gap profile is given by

$$\tilde{h}(\tilde{r}) = q + \tfrac{1}{2}\tilde{r}^2. \tag{B6}$$

The permeability function is given by

$$g(q) = \frac{1}{8}\int_0^{\infty}(\tilde{w}_{\infty} - \tilde{w})r^4\,\mathrm{d}r, \tag{B7}$$

and $\tilde{w}_{\infty}$ corresponds to (3.16),

$$\tilde{w}_{\infty} = \tilde{w}\left[\tilde{P}_{\infty}\right] = \frac{12\tilde{r}}{5}\frac{\tilde{r}^2 - 4}{\tilde{h}^4}. \tag{B8}$$

The permeability-scaled Reynolds equation (B3) has regular perturbation solution for $q \ll 1$,

$$\tilde{w}(\tilde{r}, q) = \tilde{w}_0(\tilde{r}) + O(q), \tag{B9}$$

where $\tilde{w}_0(\tilde{r})$ is the solution with $q = 0$, corresponding to a contact configuration of the particles. Inserting this expansion into the Reynolds equation (B3) yields the leading-order

938 A27-26

behaviour

$$g(q) = \frac{1}{8} \int_0^\infty (\tilde{w}_\infty - \tilde{w}_0) r^4 \, dr + O(q). \tag{B10}$$

For convenience, this is rewritten as,

$$g(q) = \frac{1}{8} \int_0^1 \tilde{w}_\infty r^4 \, dr - \frac{1}{8} \int_0^1 \tilde{w}_0 r^4 \, dr + \frac{1}{8} \int_1^\infty (\tilde{w}_\infty - \tilde{w}_0) r^4 \, dr + O(q), \tag{B11}$$

to isolate the log-singular behaviour resulting from the integration of $\tilde{w}_\infty(\tilde{r})$ at $r = 0$. Up to $O(1)$, formula (3.17) was obtained by a numerical solution of $\tilde{w}_0$ and evaluation of integrals in (B11); the $O(q)$ coefficient was obtained by fitting to the solution at finite q.

B.2. *Large q limit*

For $q \gg 1$, the solution of (3.10) has the form of a regular perturbation

$$\hat{w}(\hat{r}, q) = \hat{w}_\infty(\hat{r}) + q^{-5/2} \hat{w}_1(\hat{r}) + O(q^{-5}), \tag{B12}$$

where $\hat{w}_\infty(\hat{r})$ is given by (3.16). At leading order for large q, the transverse permeability function (3.14) is given by

$$g(q) = -\frac{1}{8} q^{-5/2} \int_0^\infty \hat{w}_1 r^4 \, dr + O(q^{-5}), \tag{B13}$$

where the first-order correction field, $\hat{w}_1(\hat{r})$, satisfies

$$\frac{1}{12} \hat{w}_1 \hat{h}^3 + \frac{1}{4} \left(\hat{I}_A \left[\hat{w}_1 \right] + \hat{I}_B \left[\hat{w}_1 \right] \right) \hat{h}^2 \hat{r} = 2q^{-5/2} \hat{J} \left[\hat{w}_\infty \right]. \tag{B14}$$

Formula (3.18) was obtained by a numerical solution of this equation and evaluation of integral (B13).

Appendix C. Resistance functions

A brief summary of the equations needed for the full description of the resistance problem is presented in this appendix. Due to the linearity of the Stokes equations, forces, $\boldsymbol{F}_\alpha$, torques, $\boldsymbol{T}_\alpha$, and stresslets, $\boldsymbol{S}_\alpha$, exerted by a particle $\alpha = 1, 2$ on the surrounding fluid are related to its imposed motion through a resistance matrix (Jeffrey & Onishi 1984a; Jeffrey 1992; Kim & Karrila 2005),

$$\begin{pmatrix} F_1 \\ F_2 \\ T_1 \\ T_2 \\ S_1 \\ S_2 \end{pmatrix} = \mu \begin{pmatrix} A_{11} & A_{12} & \tilde{B}_{11} & \tilde{B}_{12} & \tilde{G}_{11} & \tilde{G}_{12} \\ A_{21} & A_{22} & \tilde{B}_{21} & \tilde{B}_{22} & \tilde{G}_{21} & \tilde{G}_{22} \\ B_{11} & B_{12} & C_{11} & C_{12} & \tilde{H}_{11} & \tilde{H}_{12} \\ B_{21} & B_{22} & C_{21} & C_{22} & \tilde{H}_{21} & \tilde{H}_{22} \\ G_{11} & G_{12} & H_{11} & H_{12} & M_{11} & M_{12} \\ G_{21} & G_{22} & H_{21} & H_{22} & M_{21} & M_{22} \end{pmatrix} \begin{pmatrix} U_1 - U_\infty(r_1) \\ U_2 - U_\infty(r_2) \\ \omega_1 - \omega_\infty \\ \omega_2 - \omega_\infty \\ -E_\infty \\ -E_\infty \end{pmatrix}, \tag{C1}$$

where $\boldsymbol{A}$, $\boldsymbol{B}$, $\tilde{\boldsymbol{B}}$ and $\boldsymbol{C}$ are second-order tensors; $\boldsymbol{G}$, $\tilde{\boldsymbol{G}}$, $\boldsymbol{H}$ and $\tilde{\boldsymbol{H}}$ are third-order tensors; and $\boldsymbol{M}$ is a fourth-order tensor that is irrelevant for rigid particles; μ is the fluid viscosity.

The spheres have linear and angular velocities U_α and ω_α, respectively, and are immersed in a linear ambient flow field

$$U_\infty(r) = U_0 + E_\infty \cdot r + \omega_\infty \times r, \tag{C2}$$

where r is the position vector and the centres of the spheres are at r_α. The quantities E_∞, ω_∞ and U_0 are, respectively, the rate of strain and vorticity in the fluid, and the velocity at $r = 0$. The resistance matrix (D1*a,b*) is symmetric and positive definite by the Lorentz reciprocal theorem.

Dimensionless resistance tensors, denoted with a hat, are defined (Jeffrey & Onishi 1984*a*; Jeffrey 1992)

$$A_{\alpha\beta} = 3\pi(a_\alpha + a_\beta)\hat{A}_{\alpha\beta}, \tag{C3a}$$

$$B_{\alpha\beta} = \pi(a_\alpha + a_\beta)^2\hat{B}_{\alpha\beta}, \tag{C3b}$$

$$C_{\alpha\beta} = \pi(a_\alpha + a_\beta)^3\hat{C}_{\alpha\beta}, \tag{C3c}$$

$$G_{\alpha\beta} = \pi(a_\alpha + a_\beta)^2\hat{G}_{\alpha\beta}, \tag{C3d}$$

$$H_{\alpha\beta} = \pi(a_\alpha + a_\beta)^3\hat{H}_{\alpha\beta}, \tag{C3e}$$

$$M_{\alpha\beta} = (5/6)\pi(a_\alpha + a_\beta)^3\hat{M}_{\alpha\beta}, \tag{C3f}$$

where α, $\beta = 1$ or 2 indicates particle labelling. The tensors obey symmetry relations that are inherent to the geometry of the two-sphere configuration. For spherical particles, the resistance tensors can be decomposed into, at most, two scalar functions $X_{\alpha\beta}^R$ and $Y_{\alpha\beta}^R$ that denote particle resistances parallel and perpendicular to the line of centres of the pair. By symmetry, only two resistance functions, i.e. X_{11}^R and X_{21}^R or Y_{11}^R and Y_{21}^R, are needed (cf. Jeffrey & Onishi (1984*a*, (1.9)) and Jeffrey (1992, (5))). Here, R refers to one of the resistance tensors.

C.1. *Transverse resistance functions*

The resistance functions for hard spheres were evaluated by setting $\bar{R}_0 = c/\sqrt{\xi}$ in integrals (2.30*a,b*), where c is a constant. The result is

$$I_1 = \tfrac{12}{5}(1 + \kappa^{-1})^{-2}\log\xi^{-1} + C_1, \quad I_2 = (1 + \kappa^{-1})^{-1}\log\xi^{-1} + C_2, \tag{C4a,b}$$

where C_1 and C_2 depend on size ratio. Then inserting these results in (2.23)–(2.28), setting the permeability integral $I_K = 0$ and collecting all non-singular terms into the matching constants $R_{\alpha\beta}^Y$ yields

$$Y_{11}^{A,0} = \frac{4}{15}\frac{\kappa(2 + \kappa + 2\kappa^2)}{(1 + \kappa)^3}\log\xi^{-1} + A_{11}^Y(\kappa), \tag{C5}$$

$$Y_{21}^{A,0} = -\frac{8}{15}\frac{\kappa(2 + \kappa + 2\kappa^2)}{(1 + \kappa)^4}\log\xi^{-1} + A_{21}^Y(\kappa), \tag{C6}$$

$$Y_{11}^{B,0} = -\frac{1}{5}\frac{\kappa(4+\kappa)}{(1+\kappa)^2}\log\xi^{-1} + B_{11}^{Y}(\kappa), \tag{C7}$$

$$Y_{21}^{B,0} = -\frac{4}{5}\frac{\kappa^2(1+4\kappa)}{(1+\kappa)^4}\log\xi^{-1} + B_{21}^{Y}(\kappa), \tag{C8}$$

$$Y_{11}^{C,0} = \frac{2}{5}\frac{\kappa}{1+\kappa}\log\xi^{-1} + C_{11}^{Y}(\kappa), \tag{C9}$$

$$Y_{21}^{C,0} = \frac{4}{5}\frac{\kappa^2}{(1+\kappa)^4}\log\xi^{-1} + C_{21}^{Y}(\kappa), \tag{C10}$$

$$Y_{11}^{G,0} = \frac{1}{10}\frac{\kappa(4-\kappa+7\kappa^2)}{(1+\kappa)^3}\log\xi^{-1} + G_{11}^{Y}(\kappa), \tag{C11}$$

$$Y_{21}^{G,0} = \frac{2}{5}\frac{\kappa^2(7-\kappa+4\kappa^2)}{(1+\kappa)^5}\log\xi^{-1} + G_{21}^{Y}(\kappa), \tag{C12}$$

$$Y_{11}^{H,0} = \frac{1}{10}\frac{\kappa(2-\kappa)}{(1+\kappa)^2}\log\xi^{-1} + H_{11}^{Y}(\kappa), \tag{C13}$$

$$Y_{21}^{H,0} = \frac{2}{5}\frac{\kappa^2(7+\kappa)}{(1+\kappa)^5}\log\xi^{-1} + H_{21}^{Y}(\kappa). \tag{C14}$$

The matching constants $R_{\alpha\beta}^{Y}$ depend only on size-ratio and are tabulated in the literature for a limited set of size ratios (O'Neill & Majumdar 1970*a*,*b*; Jeffrey & Onishi 1984*a*; Corless & Jeffrey 1988*b*; Kim & Karrila 2005); herein, we used the code developed by D.J. Jeffrey to generate these constants (https://www.uwo.ca/apmaths/faculty/jeffrey/).

C.2. *Axisymmetric resistance functions*

For axisymmetric motion of spheres, there is no coupling between rotation and translation or strain thus, $\boldsymbol{B} = \tilde{\boldsymbol{B}} = 0$, and $\boldsymbol{H} = \tilde{\boldsymbol{H}} = 0$. The leading-order, resistance functions for hard spheres in translation and strain are (Cooley & O'Neill 1969*b*,*a*; Jeffrey & Onishi 1984*a*; Corless & Jeffrey 1988*b*; Jeffrey 1992; Kim & Karrila 2005)

$$X_{11}^{A,0} = \frac{2\kappa^2}{(1+\kappa)^3}\xi^{-1} + O\left(\log\xi^{-1}\right), \tag{C15}$$

$$X_{21}^{A,0} = -\frac{4\kappa^2}{(1+\kappa)^4}\xi^{-1} + O\left(\log\xi^{-1}\right), \tag{C16}$$

$$X_{11}^{G,0} = \frac{3\kappa^2}{(1+\kappa)^3}\xi^{-1} + O\left(\log\xi^{-1}\right), \tag{C17}$$

and

$$X_{21}^{G,0} = \frac{12\kappa^3}{(1+\kappa)^5}\xi^{-1} + O\left(\log\xi^{-1}\right). \tag{C18}$$

As indicated, these resistances have a ξ^{-1} singularity at contact. The other non-zero elements of the axisymmetric resistance matrix are the non-singular rotational

resistances

$$X_{11}^{C,0} = \frac{\kappa^3}{(1+\kappa)^3}\zeta\left(3,\frac{\kappa}{1+\kappa}\right) + O\left(\xi\log\xi^{-1}\right), \tag{C19}$$

$$X_{21}^{C,0} = -\frac{8\kappa^3}{(1+\kappa)^6}\zeta(3,0) + O\left(\xi\log\xi^{-1}\right), \tag{C20}$$

where $\zeta(z,p) = \sum_{k=0}^{\infty}(k+p)^{-z}$ is the Riemann-zeta function.

Appendix D. Axisymmetric lubrication resistance

The axisymmetric integro-differential Reynolds lubrication equation, analogous to (3.6a), has been derived elsewhere (Reboucas & Loewenberg 2021a, (3.6)) and the axisymmetric permeability function analysed. For completeness, the principal results are provided in this appendix. Except as noted, local variable definitions are used. The integral form of the axisymmetric Reynolds lubrication equation, presented below, is closely analogous to the transverse Reynolds lubrication (3.10), except that the pressure has no angular dependence and the pressure and flux scalings in variables (3.4a–d) are given by

$$\hat{p} = \frac{pL_0^4}{\mu Wa^3}, \quad \hat{J} = \frac{J}{W}q^{5/2}, \tag{D1a,b}$$

where $W = U_{z_1} - U_{z_2}$ is the relative velocity of the particles along their line of centres, and L_0 is the geometric length scale (3.5).

The integral form of the axisymmetric Reynolds lubrication equation is

$$\tfrac{1}{12}\hat{w}\hat{h}^3 + \tfrac{1}{4}\hat{I}_A\left[\hat{w}\right]\hat{h}^2 - 2q^{-5/2}\hat{J}\left[\hat{w}\right] = -1, \tag{D2}$$

where $\hat{h}$ is defined by (3.7)

$$\hat{w}(\hat{r}) = \frac{1}{\hat{r}}\left(\hat{r}\hat{p}'\right)', \quad \text{and} \quad \hat{I}_A\left[\hat{w}\right] = \int_0^{\hat{r}}\hat{w}r\,\mathrm{d}r. \tag{D3a,b}$$

The intraparticle flux, $\hat{J}$, is given by (3.8) with Green's function

$$\phi(x) = \frac{2}{\pi}\frac{x}{1+x}\mathrm{K}\left(\frac{2\sqrt{x}}{1+x}\right), \tag{D4}$$

where $x = r/\hat{r}$, and K is the first-kind elliptic integral defined by (A16a). The axisymmetric permeability function $f(q)$ is given by

$$f(q) = \frac{1}{3}\int_0^{\infty}\hat{p}r\,\mathrm{d}r = \frac{1}{12}\int_0^{\infty}\hat{w}r^3\,\mathrm{d}r. \tag{D5}$$

The numerical procedure described in §3.1 was used to solve (D2). The results for $f(q)$ are shown graphically in figure 2 and provided in tabular form in the Supplementary Material. An analysis for small and large values of q, similar to that presented in §3.2,

yields (Reboucas & Loewenberg 2021a)

$$f(q) = b_1 q - b_2 q^2 + O(q^3), \quad q \ll 1, \tag{D6}$$

with $b_1 \doteq 0.7507$ and $b_2 \doteq 0.224$, and

$$f(q) = 1 - c_1 q^{-5/2} + O(q^{-5}), \quad q \gg 1, \tag{D7}$$

with $c_1 \doteq 1.8402$. For hard spheres, $\hat{p} = 3\hat{h}^{-2}$ and thus $f = 1$. Accordingly, these results show that permeability reduces the lubrication pressure for axisymmetric near-contact motion.

Appendix E. Near-contact axisymmetric mobility functions

In the near-contact regime, the axisymmetric mobility functions L and A are proportional to the G mobility function for permeable spheres (5.7), as indicated by (5.11). Here, the calculation of the contact forces is described and a table of values is provided.

The contact forces are made dimensionless as

$$\hat{F}_c^{(g)} = \frac{F_c^{(g)}}{6\pi\mu a U_{12,g}^\infty}, \quad \hat{F}_c^{(E)} = \frac{F_c^{(E)}}{6\pi\mu a U_{12,E}^\infty}, \tag{E1a,b}$$

where $U_{12,g}^\infty$ is defined by (5.2a,b), and

$$U_{12,E}^\infty = E\bar{a}(1 - A), \tag{E2}$$

is the relative velocity along the line of centres of two spheres in an extensional flow, where $\bar{a}$ is the average radius and E is the rate of strain.

The contact forces are obtained from a force balance on the particles, taking account of the drag forces due to pair migration, gravity forces or forces exerted by the axisymmetric straining flow. The results are (Cooley & O'Neill 1969a; Nir & Acrivos 1973)

$$\hat{F}_c^{(g)} = \frac{\kappa^{-1} + 1}{\kappa^2\gamma - 1}\left[\frac{R_2 - R_1\kappa^3\gamma}{R_1 + R_2}\right], \tag{E3}$$

and

$$\hat{F}_c^{(E)} = \frac{1}{\kappa}\frac{R_2^{(E)}R_1 - R_1^{(E)}R_2}{R_1 + R_2}, \tag{E4}$$

where

$$R_1 = A_{11}^X + \frac{1+\kappa}{2}A_{12}^X, \tag{E5}$$

$$R_2 = \kappa A_{22}^X + \frac{1+\kappa}{2}A_{12}^X, \tag{E6}$$

$$R_1^{(E)} = A_{11}^X - \frac{\kappa(1+\kappa)}{2}A_{12}^X - \frac{2}{3}G_{11}^X - \frac{(1+\kappa)^2}{6}G_{21}^X + (1+\kappa^{-1})^{-2}, \tag{E7}$$

and

$$R_2^{(E)} = \frac{1+\kappa}{2}A_{12}^X - \kappa^2 A_{22}^X - \frac{(1+\kappa)^2}{6}G_{12}^X + \frac{2}{3}\kappa^2 G_{22}^X - (1+\kappa^{-1})^{-2}. \tag{E8}$$

In (E5)–(E8), $A_{\alpha\beta}^X$ and $G_{\alpha\beta}^X$ are matching constants for the axisymmetric resistance functions, $X_{\alpha\beta}^A$ and $X_{\alpha\beta}^G$, obtained from the resistance matrix (C1). For convenience, representative values of the contact forces are provided in table 6.

κ	1	0.9	0.75	0.6	0.5	0.4	0.3	0.25	0.125
$\hat{F}_c^{(g)}$	—	0.3862	0.3673	0.3256	0.2825	0.2270	0.1611	0.1260	0.04296
$\hat{F}_c^{(E)}$	2.038	2.024	1.933	1.730	1.518	1.238	0.8982	0.7123	0.2538

Table 6. Contact forces for particles migrating in gravity ($\gamma = 1$) and in axisymmetric straining flow.

REFERENCES

AURIAULT, J.L. 2009 On the domain of validity of Brinkman's equation. *Transp. Porous Media* **79**, 215–223.

BÄBLER, M.U., SEFCIK, J., MORBIDELLI, M. & BALDYGA, J. 2006 Hydrodynamic interactions and orthokinetic collisions of porous aggregates in the Stokes regime. *Phys. Fluids* **18**, 013302.

BARS, M.L. & WOSTER, M.G. 2006 Interfacial conditions between a pure fluid and a porous medium: implications for binary alloy solidification. *J. Fluid Mech.* **550**, 149–173.

BATCHELOR, G.K. 1982 Sedimentation in a dilute polydisperse system of interacting spheres. Part 1. General theory. *J. Fluid Mech.* **119**, 379–408.

BATCHELOR, G.K. & GREEN, J.T. 1972 The hydrodynamic interaction of two small freely-moving spheres in a linear flow field. *J. Fluid Mech.* **56** (2), 375–400.

BATCHELOR, G.K. & O'BRIEN, R.W. 1977 Thermal or electrical conduction through a granular material. *Proc. R. Soc. Lond.* A **355** (1682), 313–333.

BEAVERS, G.S. & JOSEPH, D.D. 1967 Boundary conditions at a naturally permeable wall. *J. Fluid Mech.* **30**, 197–207.

BELFORT, G., DAVIS, R.H. & ZYDNEY, A.L. 1994 The behavior of suspensions and macromolecular solutions in crossflow microfiltration. *J. Memb. Sci.* **96**, 1–58.

BLUE, L.E. & JORGENSON, J.W. 2015 1.1 µm superficially porous particles for liquid chromatography. Part II. Column packing and chromatographic performance. *J. Chromatogr.* A **1380**, 71–80.

BRENNER, H. 1961 The slow motion of a sphere through a viscous fluid towards a plane surface. *Chem. Engng Sci.* **16** (3-4), 242–251.

BRENNER, H. & O'NEILL, M.E. 1972 On the Stokes resistance of multiparticle systems in a linear shear field. *Chem. Engng Sci.* **27** (7), 1421–1439.

BRINKMAN, H.C. 1949 A calculation of the viscous force exerted by a flowing fluid on a dense swarm of particles. *Appl. Sci. Res.* A **1**, 27–34.

BURGANOS, V.N., MICHALOPOULOU, A.C., DASSIOS, G. & PAYATAKES, A.C. 1992 Creeping flow around and through a permeable sphere moving with constant velocity towards a solid wall: a revision. *Chem. Engng Commun.* **117**, 85–88.

CAO, Y., GUNZBURGER, M., HUA, F. & WANG, X. 2010 Coupled Stokes-Darcy model with Beavers-Joseph interface boundary condition. *Commun. Math. Sci.* **8**, 1–25.

CHEN, S.B. 1998 Axisymmetric motion of multiple composite spheres: solid core with permeable shell, under creeping flow conditions. *Phys. Fluids* **10**, 1150.

CHEN, S.B. & CAI, A. 1999 Hydrodynamic interactions and mean settling velocity of porous particles in a dilute suspension. *J. Colloid Interface Sci.* **217**, 328–340.

CHILDRESS, S. 1972 Viscous flow past a random array of spheres. *J. Chem. Phys.* **56** (6), 2527–2539.

CIVAN, F. 2007 Reservoir Formation Damage, 2nd edn, chap. 18. Elsevier.

COOLEY, M.B.A. & O'NEILL, M.E. 1968 On the slow rotation of a sphere about a diameter parallel to a nearby plane wall. *IMA J. Appl. Maths* **4** (2), 163–173.

COOLEY, M.B.A. & O'NEILL, M.E. 1969a On the slow motion of two spheres in contact along their line of centres through a viscous fluid. *Math. Proc. Camb. Phil. Soc.* **66** (2), 407–415.

COOLEY, M.D.A. & O'NEILL, M.E. 1969b On the slow motion generated in a viscous fluid by the approach of a sphere to a plane wall or stationary sphere. *Mathematika* **16** (1), 37–49.

CORLESS, R.M. & JEFFREY, D.J. 1988a Forces and stresslets for the axisymmetric motion of nearly touching unequal spheres. *Physico-Chem. Hydrodyn.* **10**, 461–470.

CORLESS, R.M. & JEFFREY, D.J. 1988b Stress moments of nearly touching spheres in low Reynolds number flow. *Z. Angew. Math. Phys.* **39**, 874–884.

DAMIANO, E.R., LONG, D.S., EL-KHATIB, F.H. & STACE, T.M. 2004 On the motion of a sphere in a stokes flow parallel to a brinkman half-space. *J. Fluid Mech.* **500**, 75–101.

DARCY, H. 1856 *Les Fontaines Publiques de la Ville de Dijon*. Dalmont.

DAVIS, A.M.J. 2001 Axisymmetric flow due to a porous sphere sedimenting towards a solid sphere or a solid wall: application to scavanging of small particles. *Phys. Fluids* **13**, 3126.

DAVIS, R.H. & STONE, H.A. 1993 Flow through beds of porous particles. *Chem. Engng Sci.* **48** (23), 3993–4005.

DAVIS, R.H., SCHONBERG, J.A. & RALLISON, J.M. 1989 The lubrication force between two viscous drops. *Phys. Fluids* A **1** (1), 77–81.

DEBBECH, A., ELASMI, L. & FEUILLEBOIS, F. 2010 The method of fundamental solution for the creeping flow around a sphere close to a membrane. *Z. Angew. Math. Mech.* **90** (12), 920–928.

DURLOFSKY, L. & BRADY, J.F. 1987 Analysis of the Brinkman equation as a model for flow in porous media. *Phys. Fluids* **30** (11), 3329–3341.

GOLDMAN, A.J., COX, R.G. & BRENNER, H. 1967a Slow viscous motion of a sphere parallel to a plane wall–I. Motion through a quiescent fluid. *Chem. Engng Sci.* **22** (4), 637–651.

GOLDMAN, A.J., COX, R.G. & BRENNER, H. 1967b Slow viscous motion of a sphere parallel to a plane wall–II. Couette flow. *Chem. Engng Sci.* **22** (4), 653–660.

GOREN, S.L. 1979 The hydrodynamic force resisting the approach of a sphere to a plane permeable wall. *J. Colloid Interface Sci.* **69**, 78–85.

HAPPEL, J. & BRENNER, H. 1983 *Low Reynolds Number Hydrodynamics*. Springer.

HERTZ, H. 1882 Ueber die berührung fester elastischer körper. [On the fixed elastic body contact]. *J. Reine Angew. Math.* **92**, 156–171.

HOWELLS, I.D. 1974 Drag due to the motion of a Newtonian fluid through a sparse random array of small fixed rigid objects. *J. Fluid Mech.* **64** (3), 449–476.

HWANG, K.J. & SZ, P.Y. 2011 Membrane fouling mechanism and concentration effect in cross-flow microfiltration of BSA/dextran mixtures. *Chem. Engng J.* **166**, 669–677.

INGBER, M.S. & ZINCHENKO, A. 2012 Semi-analytic solution of the motion of two spheres in arbitrary shear flow. *Intl J. Multiphase Flow* **42**, 152–163.

JEFFREY, D.J. 1982 Low-Reynolds-number flow between converging spheres. *Mathematika* **29** (1), 58–66.

JEFFREY, D.J. 1989 Higher–order corrections to the axisymmetric interactions of nearly touching spheres. *Phys. Fluids* A **1** (10), 1740–1742.

JEFFREY, D.J. 1992 The calculation of the low Reynolds number resistance functions for two unequal spheres. *Phys. Fluids* A **4** (1), 16–29.

JEFFREY, D.J. & ONISHI, Y. 1984a The forces and couples acting on two nearly touching spheres in low-Reynolds-number flow. *Z. Angew. Math. Phys.* **35**, 634–641.

JEFFREY, D.J. & ONISHI, Y. 1984b Calculation of the resistance and mobility functions for two unequal rigid spheres in low-Reynolds-number flow. *J. Fluid Mech.* **139**, 261–290.

JONES, R.B. 1978 Hydrodynamic interactions of two permeable spheres I: the method of reflections. *Physica* A **92**, 545–556.

KHABTHANI, S., SELLIER, A. & FEUILLEBOIS, F. 2019 Lubricating motion of a sphere towards a thin porous slab with Saffman slip condition. *J. Fluid Mech.* **867**, 949–968.

KIM, S. & KARRILA, S.J. 2005 *Microhydrodynamics: Principles and Selected Applications*. Dover.

KIM, S. & MIFFLIN, R.T. 1985 The resistance and mobility functions of two equal spheres in low-Reynolds-number flow. *Phys. Fluids* **28** (7), 2033–2045.

LE-CLECH, P., CHEN, V. & FANE, T.A.G. 2006 Fouling in membrane bioreactors used in wastewater treatment. *J. Memb. Sci.* **284**, 17–53.

LÉVY, T. 1983 Fluid flow through an array of fixed particles. *Intl J. Engng Sci.* **21** (1), 11–23.

LIAPIS, A.I. & MCCOY, M.A. 1994 Perfusion chromatography: effect of micropore diffusion on column performance in systems utilizing perfusive adsorbent particles with a bidisperse porous structure. *J. Chromatogr.* A **660** (1), 85–96.

LIN, C.J., LEE, K.J. & SATHER, N.F. 1970 Slow motion of two spheres in a shear field. *J. Fluid Mech.* **43** (1), 35–47.

MAUDE, A.D. 1963 The movement of a sphere in front of a plane at low Reynolds number. *Brit. J. Appl. Phys.* **14** (12), 894.

MICHALOPOULOU, A.C., BURGANOS, V.N. & PAYATAKES, A.C. 1992 Creeping axisymmetric flow around a solid particle near a permeable obstacle. *AIChE J.* **38**, 1213–1228.

MICHALOPOULOU, A.C., BURGANOS, V.N. & PAYATAKES, A.C. 1993 Hydrodynamic interactions of two permeable particles moving slowly along their centerline. *Chem. Engng Sci.* **48**, 2889–2900.

NEALE, G. & NADER, W. 1974 Practical significance of Brinkman's extension of Darcy's law: coupled parallel flows within a channel and a bounding porous medium. *Can. J. Chem. Engng* **52**, 475–478.

NIR, A. 1981 On the departure of a sphere from contact with a permeable membrane. *J. Engng Maths* **15**, 65–75.

NIR, A. & ACRIVOS, A. 1973 On the creeping motion of two arbitrary-sized touching spheres in a linear shear field. *J. Fluid Mech.* **59** (2), 209–223.

OCHOA-TAPIA, J.A. & WHITAKER, S. 1995 Momentum transfer at the boundary between a porous medium and a homogeneous fluid. I. Theoretical development. *Intl J. Heat Mass Transfer* **38**, 2635–2646.

O'NEILL, M.E. & MAJUMDAR, R. 1970*a* Asymmetrical slow viscous fluid motions caused by the translation or rotation of two spheres. Part 1. The determination of exact solutions for any values of the ratio of radii and separation parameters. *Z. Angew. Math. Phys.* **21**, 164–179.

O'NEILL, M.E. & MAJUMDAR, R. 1970*b* Asymmetrical slow viscous fluid motions caused by the translation or rotation of two spheres. Part 2. Asymptotic forms of the solutions when the minimum clearance between the spheres approaches zero. *Z. Angew. Math. Phys.* **21**, 180–187.

O'NEILL, M.E. & STEWARTSON, K. 1967 On the slow motion of a sphere parallel to a nearby plane wall. *J. Fluid Mech.* **27** (4), 705–724.

PAYATAKES, A.C. & DASSIOS, G. 1987 Creeping flow around and through a permeable sphere moving with constant velocity towards a solid wall. *Chem. Engng Commun.* **58**, 119–138.

RAMON, G.Z. & HOEK, E.M.V. 2012 On the enhanced drag force induced by permeation through a filtration membrane. *J. Memb. Sci.* **392–393**, 1–8.

RAMON, G.Z., HUPPERT, H.E., LISTER, J.R. & STONE, H.A. 2013 On the hydrodynamic interaction between a particle and a permeable surface. *Phys. Fluids* **25**, 073103.

REBOUCAS, R.B. & LOEWENBERG, M. 2021*a* Near-contact approach of two permeable spheres. *J. Fluid Mech.* **925**, A1.

REBOUCAS, R.B. & LOEWENBERG, M. 2021*b* Collision rates of permeable particles in creeping flows. *Phys. Fluids* **33**, 083322.

RODRIGUES, A.E., AHN, B.J. & ZOULALIAN, A. 1982 Intraparticle-forced convection effect in catalyst diffusivity measurements and reactor design. *AIChE J.* **28** (4), 541–546.

ROY, B.C. & DAMIANO, E.R. 2008 On the motion of a porous sphere in a stokes flow parallel to a planar confining boundary. *J. Fluid Mech.* **606**, 75–104.

SAFFMAN, P.G. 1971 On the boundary condition at the surface of a porous medium. *Stud. Appl. Maths* **50**, 93–101.

STIMSON, M. & JEFFERY, G.B. 1926 The motion of two spheres in a viscous fluid. *Proc. R. Soc. Lond.* A **111** (757), 110–116.

TAM, C.K.W. 1969 The drag on a cloud of spherical particles in low Reynolds number flow. *J. Fluid Mech.* **38** (3), 537–546.

WANG, J., CAHYADI, A., WU, B., PEE, W., FANE, A.G. & CHEW, J.W. 2020 The roles of particles in enhancing membrane filtration: a review. *J. Memb. Sci.* **595**, 117570.